

1 **Molecular corridors and kinetic regimes in the multiphase chemical evolution of**  
2 **secondary organic aerosol**

3

4 Manabu Shiraiwa<sup>1,\*</sup>, Thomas Berkemeier<sup>1</sup>, Katherine A. Schilling-Fahnestock<sup>2</sup>, John  
5 H. Seinfeld<sup>2</sup> & Ulrich Pöschl<sup>1</sup>

6

7

8 <sup>1</sup> Multiphase Chemistry Department, Max Planck Institute for Chemistry, 55128  
9 Mainz, Germany.

10 <sup>2</sup> Division of Chemistry and Chemical Engineering, California Institute of  
11 Technology, Pasadena, CA91125, USA.

12

13

14 \* Corresponding author (m.shiraiwa@mpic.de)

15

16 Last update: 16 June 2014

17

18 To be submitted to *ACP*

19

20

21 **Abstract.**

22 The dominant component of atmospheric organic aerosol is that derived from the  
23 oxidation of volatile organic compounds (VOCs), so-called secondary organic aerosol  
24 (SOA). SOA consists of a multitude of organic compounds, only a small fraction of  
25 which has historically been identified. Formation and evolution of SOA is a complex  
26 process involving coupled chemical reaction and mass transport in the gas and  
27 particle phases. Current SOA models do not embody the full spectrum of reaction and  
28 transport processes nor do they identify the dominant rate-limiting steps in SOA  
29 formation. Based on molecular identification of SOA oxidation products, we show  
30 here that the chemical evolution of SOA from a variety of VOC precursors adheres to  
31 characteristic “molecular corridors” with a tight inverse correlation between volatility  
32 and molar mass. The slope of these corridors corresponds to the increase in molar  
33 mass required to decrease volatility by one order of magnitude ( $-dM/d\log C_0$ ). It varies  
34 in the range of 10-30 g mol<sup>-1</sup> depending on the molecular size of the SOA precursor  
35 and the O:C ratio of the reaction products. Sequential and parallel reaction pathways  
36 of oxidation and dimerization or oligomerization progressing along these corridors  
37 pass through characteristic regimes of reaction-, diffusion-, or accommodation-limited  
38 multiphase chemical kinetics that can be classified according to reaction location,  
39 degree of saturation, and extent of heterogeneity of gas and particle phases. The  
40 molecular corridors and kinetic regimes help to constrain and described the properties  
41 of the products, pathways and rates of SOA evolution, thereby facilitating the further  
42 development of aerosol models for air quality and climate.

43

44 **Introduction.**

45 Organic aerosol is ubiquitous in the atmosphere and its major component is  
46 secondary organic aerosol (SOA) (Jimenez et al., 2009). Reaction of atmospheric  
47 VOCs with oxidants such as OH, O<sub>3</sub>, and NO<sub>3</sub> initiate the formation of semi-volatile  
48 organic compounds (SVOCs), which can undergo further gas-phase oxidation to form  
49 low-volatility organic compounds (LVOCs) that will preferentially partition into the  
50 particle phase (Kroll and Seinfeld, 2008; Hallquist et al., 2009; Donahue et al., 2012;  
51 Murphy et al., 2014). A fraction of the SVOCs partitions into the particle phase,  
52 wherein they can be transformed into LVOCs such as dimers, oligomers and other  
53 high molecular mass compounds (Jang et al., 2002; Kalberer et al., 2006; Ervens et  
54 al., 2011; Ziemann and Atkinson, 2012; Shiraiwa et al., 2013a). Some portion of the  
55 LVOCs can be transformed back to (semi-)volatile compounds or CO/CO<sub>2</sub> by  
56 fragmentation reactions triggered by OH or other oxidants at the particle surface or in  
57 the particle bulk (Bertram et al., 2001; Kroll and Seinfeld, 2008; Jimenez et al., 2009).  
58 SOA partitioning is also affected by particle-phase state, non-ideal thermodynamic  
59 mixing and morphology (Chang and Pankow, 2006; Zuend and Seinfeld, 2012;  
60 Shiraiwa et al., 2013b).

61 SOA consists of a myriad of organic compounds, of which only 10-30% have  
62 been identified (Goldstein and Galbally, 2007). Common techniques applied for the  
63 analysis of SOA are gas chromatography/electron impact ionization mass  
64 spectrometry (GC/EI-MS) and liquid chromatography/electrospray ionization mass  
65 spectrometry (LC/ESI-MS) (e.g., Surratt et al., 2006). Hard ionization, such as  
66 electron impact ionization, generally causes significant fragmentation of organic  
67 molecules, which makes molecular identification challenging, but can provide  
68 molecular structural information. The recent advent of soft ionization methods such as  
69 electrospray ionization (ESI), matrix-assisted laser desorption ionization (MALDI),  
70 atmospheric pressure chemical ionization (APCI), and direct analysis in real time  
71 (DART) ionization has facilitated the identification of the dominant fraction of the  
72 compounds constituting SOA by preserving analytes as intact or nearly intact during  
73 ionization (Kalberer et al., 2006; Williams et al., 2010; Laskin et al., 2012a; Laskin et  
74 al., 2012b; Chan et al., 2013; Nguyen et al., 2013; Vogel et al., 2013; Schilling-  
75 Fahnstock et al., 2014). Taking advantage of such data here we present a new 2D  
76 map for SOA evolution of molar mass vs. volatility, which can be linked to kinetic  
77 regimes and reaction pathways of formation and aging of SOA that is currently poorly

78 constrained and a major limitation in the understanding and prediction of atmospheric  
79 aerosol effects.

80

### 81 **Molecular corridors for different SOA precursors.**

82 Figure 1 shows 2D maps of molecular weight or molar mass ( $M$ ) plotted  
83 against volatility or saturation mass concentration ( $C_0$ ) for organic compounds in  
84 SOA from a range of anthropogenic and biogenic precursors: (a, b) dodecane (Yee et  
85 al., 2012), (c, d) cyclododecane, (e, f) hexylcyclohexane (Schilling-Fahnestock et al.,  
86 2014), (g)  $\alpha$ -pinene (Docherty et al., 2005; Claeys et al., 2007; Claeys et al., 2009;  
87 Zuend and Seinfeld, 2012; Kahnt et al., 2014; Kristensen et al., 2014), (h) limonene  
88 (Jaoui et al., 2006; Kundu et al., 2012), (i) isoprene (Surratt et al., 2006; Surratt et al.,  
89 2010; Lin et al., 2012; Lin et al., 2013), (j) glyoxal and methylglyoxal (Lim et al.,  
90 2010; Sareen et al., 2010; Zhao et al., 2012). Experimental conditions including  
91 oxidants, NO levels and seed particles used in earlier studies are summarized in Table  
92 A1. The experimental conditions and methods applied in this study to analyze the  
93 formation and composition of SOA from  $C_{12}$  alkanes under low- and high-NO  
94 conditions are detailed in Appendix A and Schilling-Fahnestock et al., (2014).  
95 DART is a soft ionization technique of atmospheric pressure ionization that has  
96 recently been used for the analysis of a variety of organic compounds with minimal  
97 fragmentation (Chan et al., 2013). SOA compounds identified include alcohols,  
98 ketones, aldehydes, hydroxycarbonyls, organic hydroperoxides and nitrates, which are  
99 generated in the gas phase (open markers), as well as dihydrofuran, furan, ether, ester,  
100 peroxyhemiacetal, hemiacetal, dimer, and imine, which are likely particle-phase  
101 products (Ziemann and Atkinson, 2012) (solid markers). **By the combination of an  
102 Aerosol Mass Spectrometer (AMS) and DART-MS, close to 100% identification and  
103 quantification of the particle phase for each of the three alkane systems was achieved  
104 (Schilling-Fahnestock et al., 2014). Thus, alkane SOA are plotted for low and high  
105 NO conditions in separate panels due to large number of identified products, whereas  
106 biogenic SOA data are shown in one panel due to the relatively small number of data  
107 points.**

108 Vapor pressures and saturation mass concentrations of organic compounds  
109 were estimated using the EVAPORATION model (“Estimation of vapor pressure of  
110 organics, accounting for temperature, intramolecular, and non-additivity effects”,  
111 (Comperolle et al., 2011)). The EVAPORATION model estimates vapor pressure of

112 molecules with the following functionalities: aldehyde, ketone, alcohol, ether, ester,  
113 nitrate, acid, peroxide, hydroperoxide, peroxy acyl nitrate and peracid. Organosulfates  
114 and imidazoles are not covered and were thus not included in our analysis, although  
115 they have been identified in SOA from biogenic precursors and glyoxal (Inuma et al.,  
116 2007; Surratt et al., 2008; Ervens et al., 2011).

117 The markers in Fig. 1 are color-coded with atomic O:C ratio. Generally,  
118 volatility decreases and molar mass increases with chemical aging of SOA both in the  
119 gas and particle phases. Consequently, molar mass of oxidation products tightly  
120 correlates with volatility with high coefficient of determination ( $R^2$ ) as summarized in  
121 Table 1. The 95% prediction intervals (dashed lines in Fig. 1) can be regarded as  
122 molecular corridors within which additional unidentified oxidation products are likely  
123 to fall. The negative slope of the fit lines corresponds to the increase in molar mass  
124 required to decrease volatility by one order of magnitude,  $-dM/d\log C_0$ . It increases  
125 from  $\sim 10 \text{ g mol}^{-1}$  for glyoxal and methylglyoxal to  $\sim 25 \text{ g mol}^{-1}$  for dodecane and  
126 cyclododecane, depending on the molecular size of the SOA precursor and the O:C  
127 ratio of the reaction products as will be discussed below. The mean value of  $-$   
128  $dM/d\log C_0$  averaged over all investigated systems is  $20 \pm 4 \text{ g mol}^{-1}$ .

129 The composition of SOA may vary depending not only on the organic  
130 precursor but also on the oxidant and other reaction conditions of formation and aging  
131 (Presto et al., 2005; Surratt et al., 2006; Lin et al., 2012; Lin et al., 2013; Kristensen et  
132 al., 2014; Loza et al., 2014; Xu et al., 2014). The atomic O:C ratio tends to be higher  
133 at high NO concentrations, partly due to the formation of organonitrates (Nguyen et  
134 al., 2011; Schilling-Fahnestock et al., 2014). Even though Fig. 1(g), (h), (i) contain  
135 biogenic SOA oxidation products measured under different conditions as specified in  
136 Table A1, the molecular corridors are relatively tight with  $R^2 > 0.85$ . The molecular  
137 corridors of alkane SOA formed under low and high NO conditions are also quite  
138 similar (Figs 1a-f). Thus, the molecular corridors of SOA formation appear to be  
139 determined primarily by the organic precursor, and the extent to which they are  
140 influenced by reaction conditions warrants further studies.

141

#### 142 **Kinetic regimes and limiting cases.**

143 Traditionally, SOA formation has been modeled based on instantaneous gas-  
144 particle equilibrium partitioning, implicitly assuming that gas-phase reactions are the  
145 rate-limiting step of SOA formation and growth (Pankow, 1994; Donahue et al., 2006;

146 Hallquist et al., 2009). Recent studies, however, have shown that mass transport and  
147 chemical reaction in the particle phase may also play an important role (Fig. 2)  
148 (Ervens et al., 2011; Ziemann and Atkinson, 2012; Shiraiwa et al., 2013a). Recently,  
149 Berkemeier et al. (2013) provided a conceptual framework which enables the  
150 characterization of heterogeneous reactions and gas uptake in atmospheric aerosols  
151 and clouds by a well-defined set of distinct kinetic regimes and limiting cases. We  
152 extended this framework to cover the complex interplay of gas- and particle-phase  
153 reactions in the evolution of SOA and enable a systematic classification of rate-  
154 limiting processes in the analysis and interpretation of laboratory chamber data and  
155 ambient measurements, as well as in the comparison of experimental results with  
156 theoretical predictions.

157 Different types of kinetic behavior can be characterized by three basic criteria  
158 as detailed in the Appendix B: (1) the location of the chemical reaction leading to  
159 SOA formation or aging (gas phase, particle surface, particle bulk), (2) the saturation  
160 ratio of the reactants (ratio of ambient concentration to saturation concentration), and  
161 (3) the extent of spatial heterogeneity of the gas and particle phases (concentration  
162 gradients). The kinetic regimes and limiting cases defined by these criteria can be  
163 visualized on a “kinetic cuboid”, in which each axis corresponds to one of the three  
164 classification parameters as shown in Fig. 3(a). The symbols “G”, “S”, and “B”  
165 indicate the predominant reaction location: gas phase, particle surface, or particle  
166 bulk, respectively. A subscript denotes the rate-limiting process for SOA formation  
167 and aging: “rx” indicates chemical reaction; “bd” indicates bulk diffusion; “ $\alpha$ ”  
168 indicates mass accommodation; “gd” indicates gas-phase diffusion. Depending on  
169 atmospheric composition and reaction conditions, which vary widely in space and  
170 time, the chemical evolution of organic compounds and SOA particles can progress  
171 through any of these regimes.

172 The left part of the cuboid can be regarded as a particle-phase chemistry  
173 regime and the right side as a gas-phase chemistry regime. As shown in Fig. 3(b), the  
174 particle-phase chemistry regime (SB, including surface (S) or bulk (B) reaction) can  
175 be further subdivided into a reaction-diffusion regime ( $SB^{rd}$ ), where the system is  
176 limited by reaction or diffusion in the particle-phase, and a mass-transfer regime  
177 ( $SB^{mt}$ ) limited by mass accommodation at the interface or diffusion through the gas  
178 phase (Berkemeier et al., 2013). The gas-phase chemistry regime (G) comprises the  
179 traditional scenario of SOA formation determined by a rate-limiting chemical reaction

180 in the gas phase followed by quasi-instantaneous gas-particle partitioning of the  
181 reaction products ( $G_{rx}$ ), corresponding to so-called quasi-equilibrium growth  
182 (Shiraiwa and Seinfeld, 2012; Zhang et al., 2012). The rest of the gas-phase chemistry  
183 regime is mass transport-limited and corresponds to so-called non-equilibrium growth  
184 (Perraud et al., 2012; Zaveri et al., 2014), which can be kinetically limited by gas-to-  
185 particle mass transfer (gas-phase diffusion and accommodation at the interface;  $G^{mt}$ )  
186 or retarded diffusion in the particle phase ( $G_{bd}$ ).

187

### 188 **Characteristic Pathways and Properties.**

189 Figure 4(a) shows the ensemble of molecular corridors from Fig. 1 with a total  
190 of 909 identified oxidation products from seven different SOA precursors. They are  
191 constrained by two boundary lines corresponding to the volatility of  $n$ -alkanes  
192  $C_nH_{2n+2}$  and sugar alcohols  $C_nH_{2n+2}O_n$ . These lines illustrate the regular dependence of  
193 volatility on the molar mass of organic compounds; the different slopes of  $30 \text{ g mol}^{-1}$   
194 for  $C_nH_{2n+2}$  and  $12 \text{ g mol}^{-1}$  for  $C_nH_{2n+2}O_n$  reflect that the decrease of volatility with  
195 increasing molar mass is stronger for polar compounds (see Fig. A4 for alternative  
196 representation).

197 Many early generation gas-phase oxidation products of alkanes as well as  
198 dimers or oligomers with low O:C ratio (LOC) fall into a molecular corridor close to  
199 the  $C_nH_{2n+2}$  line, which we designate as LOC corridor ( $-dM/d\log C_0 \geq \sim 25 \text{ g mol}^{-1}$ ,  
200 blue shaded area). Aqueous-phase reaction and autoxidation products with high O:C  
201 ratio (HOC), on the other hand, tend to fall into a corridor near the  $C_nH_{2n+2}O_n$  line,  
202 which we designate as HOC corridor ( $-dM/d\log C_0$  of  $\leq \sim 15 \text{ g mol}^{-1}$ , red shaded area).  
203 The area in between is characterized by intermediate O:C ratios and accordingly  
204 designated as IOC corridor ( $-dM/d\log C_0 \approx \sim 20 \text{ g mol}^{-1}$ ). Among the SOA systems  
205 investigated in this study, the small precursor VOCs glyoxal, methylglyoxal and  
206 isoprene ( $C_2$ - $C_5$ ) evolve through the HOC corridor, and the terpenes  $\alpha$ -pinene and  
207 limonene ( $C_{10}$ ) through the IOC corridor. The alkanes dodecane and cyclododecane  
208 ( $C_{12}$ ) evolve through the LOC corridor, while hexylcyclohexane exhibits a branching  
209 between the LOC and HOC corridors, suggesting the involvement of different  
210 reaction pathways. For unidentified SOA products, the molecular corridor ensemble  
211 in Fig. 4(a) and alternative representations (Fig. A4(a)) may also be used as a look-up  
212 plot to obtain a rough estimate of volatility by comparison of molar mass and O:C

213 ratio (e.g., from soft-ionization high-resolution mass spectrometry) to the data in the  
214 plot.

215 Characteristic reaction pathways and relevant kinetic regimes are outlined in  
216 Fig. 4(b). SOA precursor VOCs with high volatility and low molar mass are located  
217 in the lower right corner of the molecular corridor ensemble. As illustrated in the  
218 insert in Fig. 4(b), single-step functionalization usually leads to a small increase in  
219 molar mass, corresponding to one order of decrease in volatility (Donahue et al.,  
220 2006), while dimerization and oligomerization tend to multiply molar mass, and thus  
221 decrease volatility by multiple orders of magnitude (Trump and Donahue, 2014) (e.g.,  
222 three to four orders of magnitude for alkane and terpene SOA, see Fig. 1).  
223 Fragmentation, on the other hand, can lead to a substantial decrease of molar mass  
224 and increase in volatility (Bertram et al., 2001; Yee et al., 2012; Schilling-Fahnestock  
225 et al., 2014). As a result, simple gas-phase oxidation products are confined to the  
226 lower right area in the 2D space. Such oxidation products ( $C_0 > 10 \mu\text{g m}^{-3}$ ) tend to fall  
227 into the gas-phase reaction limiting case  $G_{\text{rx}}$  (quasi-equilibrium growth), as their gas-  
228 particle equilibration timescale is on the order of seconds to minutes (Shiraiwa and  
229 Seinfeld, 2012) (see Appendix C&D).

230 Particle-phase dimerization and oligomerization involving two or more  
231 molecules usually leads to the formation of compounds with low volatility and high  
232 molar mass lying in the upper left area in the 2D space. The formation of such  
233 particle-phase products is likely limited by reaction or diffusion in the particle bulk  
234 ( $\text{SB}^{\text{rd}}$ ), as rate coefficients for dimer formation are relatively low ( $< 10 \text{ M}^{-1} \text{ s}^{-1}$ )  
235 (Ziemann and Atkinson, 2012) and large molecules tend to diffuse slowly (Pfrang et  
236 al., 2011; Shiraiwa et al., 2011; Abramson et al., 2013; Zhou et al., 2013). An  
237 example of reaction pathways leading to dimerization is shown in Fig. 5 for dodecane  
238 SOA (Appendix D, Shiraiwa et al., 2013a). Within the molecular corridor of  
239 dodecane SOA evolution, Fig. 5 illustrates a specific trajectory from the precursor  
240 (dodecane, 0) through multiple generations of surrogate products of gas-phase  
241 oxidation and functionalization (multifunctional alcohols, ketones, and peroxides, 1-  
242 5), gas-phase fragmentation (aldehydes, 6), and particle-phase dimerization between  
243 aldehydes and peroxides to peroxyhemiacetals (7). Numerical model results shown in  
244 Fig. A2 indicate that the trajectory of chemical evolution passes through different  
245 kinetic regimes, i.e., from limitation by gas-phase reaction ( $G_{\text{rx}}$ ) to particle-phase  
246 reaction and diffusion ( $\text{SB}^{\text{rd}}$ ). Note that particle-phase reactions may also be limited



247 by gas-to-particle mass transfer (e.g., accommodation, supply of reactive gases into  
248 the particle), when they are sufficiently fast, such as catalyzed by acids (Jang et al.,  
249 2002; Iinuma et al., 2004; Offenberg et al., 2009; Surratt et al., 2010).

250 Aqueous-phase processing of glyoxal and methylglyoxal is an efficient  
251 pathway for formation of low volatility and semi-volatile HOC compounds (Liggio et  
252 al., 2005; Carlton et al., 2007; Lim et al., 2010; Ervens et al., 2011; Zhao et al., 2012).  
253 Uptake of glyoxal into the particle phase leads to hydration and acid catalysis to form  
254 hemiacetals, aldols, imines, anhydrides, esters and organosulfates (Lim et al., 2010).  
255 Reactive uptake of isoprene epoxydiols (IEPOX) and subsequent formation of  
256 oligomers (Surratt et al., 2010; Lin et al., 2012; Lin et al., 2013) also progresses over  
257 the HOC corridor. Whether multiphase chemistry of glyoxal and IEPOX is limited by  
258 mass transfer or chemical reactions may depend on various factors including reaction  
259 rate coefficients, relative humidity, particle pH, and Henry's law constant (Ervens and  
260 Volkamer, 2010; McNeill et al., 2012; Kampf et al., 2013).

261 Recently, highly oxidized extremely low volatility organic compounds  
262 (ELVOC) have been detected in field and chamber experiments (Ehn et al., 2012;  
263 Schobesberger et al., 2013; Ehn et al., 2014). Such compounds may populate the  
264 upper left corner of the HOC corridor. It has been shown that such compounds can be  
265 formed via autoxidation (inter- and intramolecular hydrogen abstraction by peroxy  
266 radicals) in the gas and particle phases (Crouse et al., 2013). When they are formed  
267 in the gas phase, the equilibration timescale of partitioning is long due to their low  
268 volatility and the SOA growth is limited most likely by mass transfer (gas-phase  
269 diffusion and accommodation;  $G^{mt}$ ) (see Appendix C and Fig. A2) (Pierce et al.,  
270 2011; Riipinen et al., 2011; Shiraiwa and Seinfeld, 2012). Note that kinetic limitation  
271 by retarded bulk diffusion ( $G_{bd}$ ) is also possible for semi-volatile and low volatility  
272 products, when organic particles adopt amorphous solid state (Virtanen et al., 2010;  
273 Cappa and Wilson, 2011; Shiraiwa et al., 2011; Vaden et al., 2011; Kuwata and  
274 Martin, 2012; Perraud et al., 2012; Shiraiwa and Seinfeld, 2012; Renbaum-Wolff et  
275 al., 2013; Zaveri et al., 2014). Indeed, recent observation found that some SVOCs do  
276 not necessarily adhere to equilibrium partitioning (Vogel et al., 2013).

277 Formation of high molecular weight SOA compounds from oligomerization or  
278 autoxidation results in high average molar mass for the biogenic systems of isoprene  
279 and  $\alpha$ -pinene (Kalberer et al., 2006) as well as the anthropogenic  $C_{12}$  alkanes (Fig. 1  
280 and Tab. 1; Schilling-Fahnestock et al., 2014). Figure 4(a) shows that most identified

281 oxidation products with molar masses higher than  $300 \text{ g mol}^{-1}$  are particle-phase  
282 products (solid markers). Thus, the relatively high average molar mass observed for  
283 laboratory-generated SOA points to the importance of particle-phase chemistry in  
284 these systems. Some SOA compounds with higher molar mass are gas-phase  
285 oxidation products including ELVOC and ester dimers observed in  $\alpha$ -pinene  
286 oxidation (Ehn et al., 2014; Kristensen et al., 2014), and there are also some particle-  
287 phase products with relatively low molar mass including furans and dihydrofurans in  
288 dodecane and cyclododecane SOA (Yee et al., 2012; Loza et al., 2014) as well as  
289 glyoxal and IEPOX products in isoprene SOA (Lim et al., 2010; Surratt et al., 2010).  
290 Nevertheless, the clustering of identified reaction products in molecular corridors may  
291 facilitate estimation of the relative importance of gas- vs. particle-phase routes to  
292 SOA formation (Fig. 1).

293 Molar mass and O:C ratio also correlate with the glass transition temperature  
294 of organic compounds, which tends to increase with increasing molar mass and O:C  
295 ratio (Koop et al., 2011). As elevated glass transition temperatures are indicative of  
296 semi-solid or amorphous solid states, SOA evolution represented in molecular  
297 corridors allows one to infer the regime, in which particles are likely to become  
298 highly viscous. For example, recent experiments have shown an order of magnitude  
299 increase in the viscosity of oleic acid particles upon reaction with ozone owing to  
300 formation of oligomers (Hosny et al., 2013), and model calculations indicate that this  
301 may lead to the formation of surface crusts (Pfrang et al., 2011).

302 In summary, presenting identified SOA products in a molecular corridor  
303 encapsulates fundamental aspects of SOA formation and aging: volatility, molar  
304 mass, O:C ratio, and phase state. Such a representation can be used to  
305 constrain/predict the properties of unidentified SOA oxidation products. The kinetic  
306 regimes, within which SOA evolution is occurring along the molecular corridor,  
307 facilitate the specification of the rate of progression to higher generation products.  
308 Thus, molecular corridors may serve as a basis for compact representation of SOA  
309 formation and aging in regional and global models of climate and air quality.

310

## 311 **Appendix A. Product analysis of alkane SOA**

312 Photo-oxidation and subsequent SOA formation of *n*-dodecane,  
313 cyclododecane, and hexylcyclohexane was conducted in the 28 m<sup>3</sup> Teflon reactors in  
314 the Caltech Environmental chamber (Yee et al., 2012; Loza et al., 2014; Schilling-  
315 Fahnestock et al., 2014). Aqueous H<sub>2</sub>O<sub>2</sub> solution was evaporated into the chamber as  
316 the OH source, followed by the atomization of an aqueous ammonium sulfate solution  
317 generating seed particles, which were subsequently dried. Experiments were  
318 conducted under low-NO conditions, in which alkyl peroxy radicals (RO<sub>2</sub>) react  
319 primarily with HO<sub>2</sub>, and under high-NO conditions, in which RO<sub>2</sub> react primarily  
320 with NO (Loza et al., 2014).

321 SOA particles were collected on Teflon filters (Pall Life Sciences, 47 mm, 1.0  
322 μm pore size). Off-line analysis of collected particles was conducted by solvent  
323 extraction and gas chromatography time-of-flight mass spectrometry (GC-TOF-MS,  
324 GCT Premier, Waters) and GC/ion trap mass spectrometry (Varian Saturn 2000,  
325 Agilent), and by direct analysis in real time (DART)- time-of-flight and ion trap mass  
326 spectrometry (DART-AccuToF, JEOL USA; Caltech Mini-DART; LTQ, Thermo  
327 Fisher). Further details on experimental conditions and analytical methods can be  
328 found in Schilling-Fahnestock et al. (2014).

329 The average molar mass of SOA was estimated by taking the sum of the  
330 product of the percent relative concentration of each compound with respect to the  
331 internal standard (dibutyl phthalate present in each filter) by each compound's molar  
332 mass. The relative concentration for each compound was obtained through the  
333 relationship of ion current intensity and concentration for DART-MS. In DART  
334 analysis, ion current intensity (*I*) is proportional to the concentration (*C*), vapor  
335 pressure (*P*<sub>vap</sub>) and proton affinity (*A*):  $I = AP_{vap}C$ . This equation is written for both  
336 the analyte and the internal standard and then the ratio was calculated, which allows  
337 for the cancellation of the proton affinity term. Analyte vapor pressures were  
338 estimated by using proposed structures based on HR-MS data-derived formulae and  
339 known mechanisms with the EVAPORATION (Estimation of vapor pressure of  
340 organics, accounting for temperature, intramolecular, and non-additivity effects)  
341 model (Compernelle et al., 2011). When rewritten to solve for the relative  
342 concentration of the analyte with respect to the concentration of the internal standard,  
343 the equation becomes:

344

$$\frac{C_A}{C_{IS}} = \frac{P_{vap,IS} I_A}{P_{vap,A} I_{IS}}$$

345

346

347

348

349

350

351

352

353

354

355

356

357

358

359

Atomic O:C ratio vs. volatility is used to represent formation and aging of SOA (Jimenez et al., 2009; Donahue et al., 2011). By analogy to Figs. 1 and 4, major oxidation products are shown in Figures S1 and S2. The markers are color coded by molar mass. Upon gas-phase oxidation, volatility decreases and O:C ratio increases, leading to a linear correlation in O:C ratio vs. volatility for gas-phase oxidation products. Particle-phase products, however, exhibit generally lower volatility and O:C ratio as compared to gas-phase oxidation products. Consequently, the overall correlation between O:C ratio and volatility for the full spectrum of SOA products has a low coefficient of determination and wide prediction interval (Table 1, Figure S1). Figure S2 shows the summary of O:C ratio vs. volatility, showing that the oxidation products cover almost the full area in this 2D space. Clear trend is found that volatile compounds have low molar mass, whereas low volatility compounds with low O:C ratio have high molar mass.

## 359 **Appendix B. Kinetic regimes for SOA formation**

360

361

362

363

364

365

366

367

368

369

370

371

372

373

374

375

376

Figure A1 shows a classification scheme for kinetic regimes and limiting cases for SOA formation and aging. Note that the term *limiting case* is reserved for a system that is governed by a single, clearly defined limiting process; the term *kinetic regime* designates a system that is governed by a few (often only one or two) clearly defined rate-limiting processes (Berkemeier et al., 2013). The classification within the particle phase regime (right-hand side of Fig. 3) is explained in detail by Berkemeier et al. (2013). In this study, the gas-phase regime (left-hand side of Fig. 3) extends the classification scheme to SOA formation. The cases of limiting behavior arise from three criteria that are fundamental to formation and partitioning of an oxidation product: 1) the location (gas phase, particle surface, particle bulk) of the reaction leading to SOA formation, 2) the species' saturation ratio (ratio of ambient concentration to saturation concentration) of the oxidation products, and 3) the extent of spatial heterogeneity of the gas and particle phases. Identifying kinetic regimes and limiting cases can be facilitated by an aerosol model, such as the kinetic multi-layer model for gas-particle interactions (KM-GAP) that explicitly resolves mass transport and chemical reactions in the gas and particle phases (Shiraiwa et al., 2012).

377 **B.1. Criterion 1: Reaction location (Gas vs. Surface vs. Bulk)**

378 *Where does formation of oxidation products that contribute to SOA mass*  
379 *predominantly occur, gas phase, particle surface or particle bulk?* A two-pronged  
380 criterion can be developed. The first sub-criterion evaluates the relative contribution  
381 of gas- vs. particle-phase chemistry. The gas- vs. particle-phase contribution ratio  
382 (GPCR) can be defined as ratio of the production rate of the oxidation product in the  
383 gas phase ( $P^g$ ) to the total production rate in gas and particle phases ( $P^g + P^p$ ):

384 
$$\text{GPCR} = P^g / (P^g + P^p) \quad (1)$$

385 As GPCR approaches unity, an oxidation product is produced primarily in the gas  
386 phase; and as GPCR approaches zero, it is primarily produced in the particle phase.

387 If particle-phase chemistry dominates ( $\text{GPCR} \approx 0$ ), the surface to total particle  
388 phase contribution ratio (STCR) is used to assess the extent to which production  
389 occurs predominantly at the surface or in the bulk. STCR can be calculated using the  
390 production rate of the oxidation product at the surface ( $P^s$ ) and in the particle bulk  
391 ( $P^b$ ):

392 
$$\text{STCR} = P^s / (P^s + P^b) \quad (2)$$

393 If the particle-phase reaction primarily occurs at the surface, STCR approaches unity;  
394 and STCR approaches zero if the reaction occurs primarily in the bulk.

395

396 **B.2. Criterion 2: Saturation ratio**

397 *Is mass transfer of an oxidation product through the gas or into the particle*  
398 *phase limiting SOA growth?* After determination of the reaction location, this  
399 criterion further classifies the system based on the abundance of oxidation products at  
400 the particle surface versus in the near-surface bulk.

401 In the gas-phase regime, the surface saturation ratio (SSR) can be used to  
402 judge the extent to which kinetic limitation of mass transport occurs in the gas phase.  
403 With this parameter, the surface concentration of an oxidation product Z,  $[Z]_s$ , is  
404 compared to its surface saturation concentration  $[Z]_{s,\text{sat}}$ . In the absence of reaction or  
405 diffusion into the bulk,  $[Z]_{s,\text{sat}}$  is determined by the gas-phase concentration of Z,  $[Z]_g$ ,  
406 and the rates of adsorption and desorption  $k_a$  and  $k_d$ :  $[Z]_{s,\text{sat}} = k_a / k_d [Z]_g$  (Pöschl et al.,  
407 2007; Berkemeier et al., 2013). The SSR is defined as the ratio of  $[Z]_s$  to its saturation  
408 concentration at adsorption equilibrium:

409 
$$\text{SSR} = [Z]_s / [Z]_{s,\text{sat}} \quad (3)$$

410 The numerical interpretation of SSR is: 1) As SSR approaches zero, the  
411 surface is starved of Z, and the system is limited by mass transfer ( $G^{mt}$  regime) either  
412 by gas-phase diffusion ( $G_{gd}$  limiting case) or surface accommodation ( $G_{\alpha}$  limiting  
413 case). As SSR approaches unity, the surface is adequately supplied with Z and the  
414 system can be limited by production of Z in the gas phase ( $G_{rx}$  limiting case) or mass  
415 transport into the bulk ( $G_{bd}$  limiting case).

416 In the particle-phase regime, the classification step is based on SSR or the  
417 bulk saturation ratio (BSR) to distinguish between systems in the reaction-diffusion  
418 regime or the mass-transfer regime (Berkemeier et al., 2013). The BSR is defined  
419 analogously to SSR as the ratio of near-surface bulk concentration of an oxidation  
420 product to its saturation concentration.

421

### 422 **B.3. Criterion 3: Mixing Parameters (MP)**

423 *Is SOA growth limited by diffusion in the gas or particle phase?* Depending on  
424 the reaction location and saturation ratio, mixing parameters are used to assess the  
425 heterogeneity of the gas-particle system. One can define the surface mixing parameter  
426 (SMP), the bulk mixing parameter (BMP), the gas-phase diffusion correction factor  
427 ( $C_g$ ), and the gas-particle mixing parameter (GMP). SMP is defined as the ratio of the  
428 actual surface concentration of compound  $i$  to the maximum possible surface  
429 concentration in the case of perfect particle-phase mixing. BMP is defined using an  
430 effective reacto-diffusive length (Berkemeier et al., 2013). As a MP approaches zero,  
431 a strong concentration gradient exists and the system is limited by diffusion; as MP  
432 approaches unity, the system is well-mixed and limited by reaction.

433 In mass-transfer limited systems (indicated by a low SR),  $C_{g,i}$  distinguishes  
434 between gas-phase diffusion limitation and accommodation limitation.  $C_{g,i}$  is defined  
435 as the ratio of the concentration of compound  $i$  in the near-surface gas phase (one  
436 mean free path away from the surface) to that in the gas phase far from the particle  
437 (Pöschl et al., 2007):

$$438 \quad C_{g,i} = C_i^{gs} / C_i^g \quad (4)$$

439 As  $C_{g,i}$  approaches zero, the compound  $i$  exhibits a strong concentration gradient in  
440 the gas phase and the system is classified as gas-phase diffusion limited ( $G_{gd}$  limiting  
441 case); as  $C_{g,i}$  approaches unity, the system is designated as accommodation-limited  
442 ( $G_{\alpha}$  limiting case).

443 The gas-particle mixing parameter (GPMP) measures the extent to which the  
 444 gas-particle system is in quasi-equilibrium and is defined as the ratio of equilibrium  
 445 gas-phase mass concentration of compound  $i$ ,  $C_i^{g,eq}$ , to gas-phase mass concentration,  
 446  $C_i^g$  (far from particle), which is equivalent to the ratio of particle-phase mass  
 447 concentration,  $C_i^{PM}$ , to equilibrium particle-phase mass concentration,  $C_i^{PM,eq}$ :

$$448 \quad GPMP_i = C_i^{g,eq} / C_i^g = C_i^{PM} / C_i^{PM,eq} \quad (5)$$

449  $C_i^{g,eq}$  and  $C_i^{PM,eq}$  can be calculated using an equilibrium partitioning theory (Pankow,  
 450 1994; Donahue et al., 2006):

$$451 \quad C_i^{g,eq} = C_i^* C_i^{PM} / C_{Tot} \quad (6)$$

$$452 \quad C_i^{PM,eq} = C_i^g C_{Tot} / C_i^* \quad (7)$$

453 where  $C_i^*$  is the effective saturation mass concentration of compound  $i$  and  $C_{Tot}$  is the  
 454 total particle mass concentration. In the case of ideal mixing,  $C_i^*$  is equal to the gas-  
 455 phase saturation mass concentration over the pure subcooled liquid ( $C_i^0$ ). Note that  
 456  $C_i^{g,eq}$  can be regarded as a gas-phase mass concentration just above the particle  
 457 surface,  $C_i^s$ , when Raoult's law is strictly obeyed and  $C_i^s$  is in equilibrium with the  
 458 whole particle (i.e., usually the case for liquid particles).

459 The value of GPMP determines the extent to which SOA growth is controlled  
 460 by quasi-equilibrium growth or mass transport limited growth.  $C_i^g = C_i^{g,eq}$  (or  $C_i^{PM} =$   
 461  $C_i^{PM,eq}$ ) at gas-particle equilibrium. The particle still grows, if  $C_i^g$  changes slowly and  
 462  $C_i^{g,eq}$  follows  $C_i^g$  instantaneously (quasi-equilibrium growth) (Shiraiwa and Seinfeld,  
 463 2012; Zhang et al., 2012). If  $C_i^g > C_i^{g,eq}$ , compound  $i$  will diffuse from the gas to the  
 464 particulate phase, driven by concentration or partial pressure gradient between the gas  
 465 and particle phases (non-equilibrium or mass transport limited growth). Thus, the  
 466 numerical interpretation of GMP is: 1) As GPMP approaches 0, SOA growth is  
 467 limited kinetically by mass transport; 2) As GPMP approaches unity, SOA growth is  
 468 in quasi-equilibrium and the system is subject to the gas-phase reaction limitation  
 469 case  $G_{rx}$  (the system is limited only by the gas-phase formation rate).

470 Note that GPMP is small for the limiting cases of  $G_{bd}$ ,  $G_\alpha$ , and  $G_{gd}$ . In these  
 471 limiting cases, SOA growth is still sensitive to the gas-phase formation rate (as it  
 472 determines the gas-phase concentration), but is limited by interfacial transport, which  
 473 comprises gas-phase diffusion, surface accommodation, and surface-to-bulk transport  
 474 processes. Gas-phase diffusion and surface accommodation limitation can be  
 475 differentiated from surface-to-bulk transport limitation either by SSR or by comparing  
 476 surface ( $\alpha_s$ ) and bulk ( $\alpha_b$ ) accommodation coefficients, each of which is resolved by

477 KM-GAP.  $\alpha_s$  is defined as the probability of a molecule sticking to the surface upon  
478 collision, whereas  $\alpha_b$  is defined as the respective probability of a molecule to enter the  
479 bulk of the particle (Pöschl et al., 2007; Shiraiwa et al., 2012). If  $\alpha_s \approx \alpha_b$ , then  
480 interfacial transport is not limited by surface-to-bulk exchange and thus is limited by  
481 either gas-phase diffusion or surface accommodation; if  $\alpha_s > \alpha_b$ , then the interfacial  
482 transport is limited by surface-to-bulk transport, (dissolution or bulk diffusion). For  
483 additional discussion of accommodation vs. surface-bulk exchange see Appendix C in  
484 Berkemeier et al. (2013).

485

### 486 **Appendix C. Examples of kinetic regimes and limiting cases**

487 Here we use KM-GAP to model condensation of a semi-volatile compound  
488 generated by oxidation of a parent VOC. We assume that the parent VOC with an  
489 initial concentration of  $10^{10} \text{ cm}^{-3}$  is converted to a semi-volatile product with a first-  
490 order rate coefficient of  $0.1 \text{ min}^{-1}$ . Conversion of the first-generation product to higher  
491 generation products and particle-phase reactions need not be considered. The initial  
492 number and mass concentrations of non-volatile pre-existing particles are taken as  $10^3$   
493  $\text{cm}^{-3}$  and  $0.1 \mu\text{g m}^{-3}$ , respectively. The initial particle size distribution is assumed log-  
494 normal with mean diameter of 50 nm and a standard deviation of 1.5. The required  
495 kinetic parameters for the simulation are given in Table A2. Gas-phase diffusion  
496 coefficient ( $D_g$ ) of an oxidation product is varied between  $0.01 - 0.05 \text{ cm}^2 \text{ s}^{-1}$  (Bilde et  
497 al., 2003; Bird et al., 2007). Surface accommodation coefficient ( $\alpha_{s,0}$ ) and bulk  
498 diffusion coefficient ( $D_b$ ) are also varied to illustrate the different kinetic regimes and  
499 limiting cases for SOA formation in the gas-phase regime.

500 Figure A2 shows the results of such simulation. The temporal evolution of  
501 mass concentration of the parent VOC (black), the oxidation product in the gas phase  
502 ( $C^g$ , solid blue), in the near-surface gas phase ( $C^{gs}$ , dotted blue), in the particle phase  
503 ( $C^{PM}$ , red), and equilibrium gas-phase concentration ( $C^{g,eq}$ , dashed blue) are shown. In  
504 the simulation presented in Figure A2a, SOA growth is limited by mass transfer,  
505 namely gas-phase diffusion and accommodation ( $G^{mt}$  regime, lying between limiting  
506 cases  $G_{gd}$  and  $G_a$ ) up to  $\sim 10$  s, indicated by a low surface saturation ratio (SSR) and a  
507 low the gas-phase diffusion correction factor ( $C_g = C^g / C^{gs} \approx 0.7$ ). The gas-phase  
508 concentration gradient vanishes within  $\sim 10$  s ( $C^g \approx C^{gs}$ ), and as  $C^g$  continues to  
509 increase due to the conversion of the parent VOC,  $C^{g,eq}$  follows the change in  $C^g$



510 essentially instantaneously and  $C^p$  increases. In this case, the gas-phase rate of  
511 formation of the oxidation product controls particle growth corresponding to the  
512 limiting case of  $G_{rx}$  (so-called quasi-equilibrium growth) (Shiraiwa and Seinfeld,  
513 2012; Zhang et al., 2012).

514 In the simulation presented in Figure A2b with a relatively low surface  
515 accommodation coefficient of  $10^{-3}$ , a steep concentration gradient exhibits between  
516 the gas phase and the particle surface ( $C^g \approx C^{gs} > C^{g,eq}$ ) during SOA growth. The  
517 system is limited by accommodation ( $G_a$ ), as SSR is low but  $C_g$  is 1. Figure A2c  
518 shows the corresponding results for particles in an amorphous semi-solid state with  
519 the low bulk diffusion coefficient of  $10^{-17} \text{ cm}^2 \text{ s}^{-1}$ . In this case, particle growth is  
520 limited by surface-to-bulk transport ( $G_{bd}$ ), as SSR is high and GPMP is low. Note that  
521 GPMP refers to the gap between  $C^g$  and  $C^{g,eq}$ . The bulk accommodation coefficient  $\alpha_b$   
522 is  $\sim 10^{-5}$ , much smaller than the surface accommodation coefficient  $\alpha_s$ . Sensitivity  
523 studies with varying  $D_b$  reveal that when  $D_b < \sim 10^{-15} \text{ cm}^2 \text{ s}^{-1}$  the timescales for  
524 surface-bulk exchange and bulk diffusion become longer than that of gas-phase  
525 diffusion and accommodation (Shiraiwa and Seinfeld, 2012). From the Stokes-  
526 Einstein relation, this value corresponds to a viscosity of  $\sim 10^7 \text{ Pa s}$ , which is on the  
527 same order as the viscosity of  $\alpha$ -pinene SOA at 40 % RH (Renbaum-Wolff et al.,  
528 2013). Thus, SOA growth can be limited by bulk diffusion at low RH; whereas  
529 surface accommodation becomes more important at high RH.

530 Figure A2d shows the simulation for gas-phase formation and partitioning of low  
531 volatility oxidation products ( $C_0 = 10^{-3} \mu\text{g m}^{-3}$ ) into liquid particles. SSR is low over  
532 the course of particle growth, indicating persistence of a strong concentration gradient  
533 between the gas phase and the particle surface. The gas-phase diffusion correction  
534 factor ( $C_g$ ) stays at 0.7 up to  $\sim 10^3 \text{ s}$ , indicating that near-surface gas phase  
535 concentration  $[Z]_{gs}$  is depleted by 30% compared to gas phase concentration  $[Z]_g$  due  
536 to rapid uptake and slow gas diffusion ( $D_g = 0.01 \text{ cm}^2 \text{ s}^{-1}$ ).  $C_g$  decreases substantially  
537 down to  $\sim 0.2$  only when gas-phase formation ceases at  $\sim 10^3 - 10^4 \text{ s}$ . Overall, SOA  
538 growth is limited by mass transfer (gas-phase diffusion and accommodation;  $G^{mt}$   
539 regime). When a very low bulk diffusivity is assumed ( $D_b \approx 10^{-19} \text{ cm}^2 \text{ s}^{-1}$ ; figure not  
540 shown), SSR is close to 1 and GPMP is very low during particle growth; thus the  
541 system is limited by bulk diffusion ( $G_{bd}$ ). Consequently, partitioning of low volatility

542 compounds could be limited by bulk diffusion, when organic particles adopt  
543 amorphous solid state (Shiraiwa and Seinfeld, 2012; Zaveri et al., 2014).

544

#### 545 **Appendix D. Application to chamber data: Dodecane photooxidation**

546 Here we apply the classification scheme to experimental data on SOA  
547 formation from oxidation of the C<sub>12</sub> alkane, dodecane (C<sub>12</sub>H<sub>28</sub>) in the Caltech  
548 Environmental Chamber (Yee et al., 2012). 34 ppb dodecane was oxidized by OH  
549 radicals over 20 hours in the presence of dry ammonium sulfate seed particles at low  
550 concentrations of NO<sub>x</sub> typical of nonurban conditions. KM-GAP was used to simulate  
551 the evolution of SOA mass, the organic atomic oxygen-to-carbon (O:C) ratio, and  
552 particle-size distribution in the chamber experiments (Shiraiwa et al., 2013a). In the  
553 gas phase, SVOCs resulting from up to five generations of OH oxidation are  
554 considered. Some of the fourth generation products have been established to be  
555 multifunctional carbonyl compounds (aldehydes) that can react in the particle phase  
556 with hydroperoxide, hydroxyl, and peroxy-carboxylic acid groups, forming  
557 peroxyhemiacetal (PHA), hemiacetal, and acylperoxyhemiacetal, respectively  
558 (Docherty et al., 2005; Yee et al., 2012; Ziemann and Atkinson, 2012). The observed  
559 evolution of the particle size distribution is simulated successfully, only if such  
560 particle-phase chemistry is included (Shiraiwa et al., 2013a).

561 Figure 5 shows the span of molar mass and gas-phase saturation  
562 concentrations over the pure subcooled liquids ( $C_i^0$ ) for gas-phase oxidation products  
563 and particle-phase products of the dodecane system. The smaller symbols indicate  
564 individual products predicted in the dodecane photooxidation chemical mechanism  
565 (Yee et al., 2012) and the large solid circles indicate the surrogate compounds used in  
566 the KM-GAP simulations (Shiraiwa et al., 2013a). Upon gas-phase multi-generation  
567 oxidation, the volatility of SVOCs decreases from  $\sim 10^6 \mu\text{g m}^{-3}$  (dodecane) to  $\sim 1 \mu\text{g}$   
568  $\text{m}^{-3}$ . The particle-phase products have significantly lower volatilities of  $\sim 10^{-2} \mu\text{g m}^{-3}$ .

569 Figures. A3a and b show the temporal evolution of mass concentration of the  
570 1<sup>st</sup> and 5<sup>th</sup> generation oxidation products in the gas phase ( $C^g$ ), at the particle surface  
571 ( $C^s$ ), and in the particle phase ( $C^{\text{PM}}$ ).  $C^g$  is slightly higher than  $C^{\text{g,eq}}$  up to  $\sim 5$  h due to  
572 continuous generation of oxidation products in the gas phase, and eventually reaching  
573  $C^g \approx C^{\text{g,eq}}$  for both products (GMP  $\approx 1$ ). Note that mass concentration in the near  
574 surface gas phase ( $C^{\text{gs}}$ ) is identical to  $C^g$ , indicating that gas-phase diffusion is not a

575 limiting step. The same trend is seen for other generation products. Thus, the  
576 contribution of gas-phase semi-volatile oxidation products to SOA formation is  
577 limited by their formation in the gas phase, corresponding to the limiting case of  $G_{rx}$ .

578 Particle-phase products are formed by the reaction of reactive aldehydes with  
579 SVOCs in the particle phase. Simulations suggest that this reaction occurs mainly at  
580 the surface and in the near-surface bulk (Shiraiwa et al., 2013a). Aldehydes and  
581 SVOCs are both saturated in the bulk (BSR is high). A strong concentration gradient  
582 of aldehydes in the bulk is predicted, whereas SVOCs are predicted to be essentially  
583 homogeneous in the bulk ( $BMP_{XY} \approx 0.5$ ). Bulk reaction is tightly coupled with bulk  
584 diffusion and the system falls into the reaction-diffusion regime ( $SB^{rd}$ ), particularly  
585 the traditional reacto-diffusive case ( $B^{rd}_{trad}$ ) (Worsnop et al., 2002; Pöschl et al., 2007;  
586 Kolb et al., 2010; Berkemeier et al., 2013).

587

#### 588 **Acknowledgements.**

589 This work was funded by the Max Planck Society and U.S. National Science  
590 Foundation grant AGS-1057183. MS, TB, and UP thank the European Commission  
591 project Pan-European gas-aerosols-climate interaction study (No. 265148,  
592 PEGASOS). MS thanks the Japan Society for the Promotion of Science (JSPS) for  
593 Postdoctoral Fellowships for Research Abroad.

594

#### 595 **References.**

596 Abramson, E., Imre, D., Beranek, J., Wilson, J. M., and Zelenyuk, A.: Experimental  
597 determination of chemical diffusion within secondary organic aerosol particles, *Phys.*  
598 *Chem. Chem. Phys.*, 15, 2983-2991, 2013.

599 Berkemeier, T., Huisman, A. J., Ammann, M., Shiraiwa, M., Koop, T., and Pöschl, U.: Kinetic  
600 regimes and limiting cases of gas uptake and heterogeneous reactions in atmospheric  
601 aerosols and clouds: a general classification scheme, *Atmos. Chem. Phys.*, 13, 6663-6686,  
602 2013.

603 Bertram, A. K., Ivanov, A. V., Hunter, M., Molina, L. T., and Molina, M. J.: The reaction  
604 probability of OH on organic surfaces of tropospheric interest, *J. Phys. Chem. A*, 105,  
605 9415-9421, 2001.

606 Bilde, M., Svenningsson, B., Monster, J., and Rosenorn, T.: Even-odd alternation of  
607 evaporation rates and vapor pressures of C3-C9 dicarboxylic acid aerosols, *Environ. Sci.*  
608 *Technol.*, 37, 1371-1378, 2003.

609 Bird, R. B., Stewart, W. E., and Lightfoot, E. N.: *Transport Phenomena* (2nd Ed.), John  
610 Wiley & Sons, Inc., New York, 2007.

- 611 Cappa, C. D., and Wilson, K. R.: Evolution of organic aerosol mass spectra upon heating:  
612 implications for OA phase and partitioning behavior, *Atmos. Chem. Phys.*, 11, 1895-  
613 1911, 2011.
- 614 Carlton, A. G., Turpin, B. J., Altieri, K. E., Seitzinger, S., Reff, A., Lim, H. J., and Ervens, B.:  
615 Atmospheric oxalic acid and SOA production from glyoxal: Results of aqueous  
616 photooxidation experiments, *Atmos. Environ.*, 41, 7588-7602, 2007.
- 617 Chan, M. N., Nah, T., and Wilson, K. R.: Real time in situ chemical characterization of sub-  
618 micron organic aerosols using Direct Analysis in Real Time mass spectrometry (DART-  
619 MS): the effect of aerosol size and volatility, *Analyst*, 138, 3749-3757, 2013.
- 620 Chang, E. I., and Pankow, J. F.: Prediction of activity coefficients in liquid aerosol particles  
621 containing organic compounds, dissolved inorganic salts, and water - Part 2:  
622 Consideration of phase separation effects by an X-UNIFAC model, *Atmos. Environ.*, 40,  
623 6422-6436, 2006.
- 624 Claeys, M., Szmigielski, R., Kourtchev, I., Van der Veken, P., Vermeylen, R., Maenhaut, W.,  
625 Jaoui, M., Kleindienst, T. E., Lewandowski, M., Offenberg, J. H., and Edney, E. O.:  
626 Hydroxydicarboxylic acids: Markers for secondary organic aerosol from the  
627 photooxidation of alpha-pinene, *Environ. Sci. Technol.*, 41, 1628-1634, 2007.
- 628 Claeys, M., Iinuma, Y., Szmigielski, R., Surratt, J. D., Blockhuys, F., Van Alsenoy, C., Boege,  
629 O., Sierau, B., Gomez-Gonzalez, Y., Vermeylen, R., Van der Veken, P., Shahgholi, M., Chan,  
630 A. W. H., Herrmann, H., Seinfeld, J. H., and Maenhaut, W.: Terpenylic Acid and Related  
631 Compounds from the Oxidation of alpha-Pinene: Implications for New Particle  
632 Formation and Growth above Forests, *Environ. Sci. Technol.*, 43, 6976-6982, 2009.
- 633 Compernelle, S., Ceulemans, K., and Muller, J. F.: EVAPORATION: a new vapour pressure  
634 estimation method for organic molecules including non-additivity and intramolecular  
635 interactions, *Atmos. Chem. Phys.*, 11, 9431-9450, 2011.
- 636 Crouse, J. D., Nielsen, L. B., Jørgensen, S., Kjaergaard, H. G., and Wennberg, P. O.:  
637 Autoxidation of organic compounds in the atmosphere, *J. Phys. Chem. Lett.*, 4, 3513-  
638 3520, 2013.
- 639 Docherty, K. S., Wu, W., Lim, Y. B., and Ziemann, P. J.: Contributions of organic peroxides  
640 to secondary aerosol formed from reactions of monoterpenes with O<sub>3</sub>, *Environ. Sci.*  
641 *Technol.*, 39, 4049-4059, 2005.
- 642 Donahue, N. M., Robinson, A. L., Stanier, C. O., and Pandis, S. N.: Coupled partitioning,  
643 dilution, and chemical aging of semivolatile organics, *Environ. Sci. Technol.*, 40, 2635-  
644 2643, 2006.
- 645 Donahue, N. M., Epstein, S. A., Pandis, S. N., and Robinson, A. L.: A two-dimensional  
646 volatility basis set: 1. organic-aerosol mixing thermodynamics, *Atmos. Chem. Phys.*, 11,  
647 3303-3318, 2011.
- 648 Donahue, N. M., Henry, K. M., Mentel, T. F., Kiendler-Scharr, A., Spindler, C., Bohn, B.,  
649 Brauers, T., Dorn, H. P., Fuchs, H., Tillmann, R., Wahner, A., Saathoff, H., Naumann, K.-H.,  
650 Möhler, O., Leisner, T., Müller, L., Reinnig, M.-C., Hoffmann, T., Salo, K., Hallquist, M.,  
651 Frosch, M., Bilde, M., Tritscher, T., Barmet, P., Praplan, A. P., DeCarlo, P. F., Dommen, J.,  
652 Prévôt, A. S. H., and Baltensperger, U.: Aging of biogenic secondary organic aerosol via  
653 gas-phase OH radical reactions, *Proc Natl Acad Sci USA*, 109, 13503-13508, 2012.

- 654 Ehn, M., Kleist, E., Junninen, H., Petaja, T., Lonn, G., Schobesberger, S., Dal Maso, M.,  
655 Trimborn, A., Kulmala, M., Worsnop, D. R., Wahner, A., Wildt, J., and Mentel, T. F.: Gas  
656 phase formation of extremely oxidized pinene reaction products in chamber and  
657 ambient air, *Atmos. Chem. Phys.*, 12, 5113-5127, 2012.
- 658 Ehn, M., Thornton, J. A., Kleist, E., Sipila, M., Junninen, H., Pullinen, I., Springer, M.,  
659 Rubach, F., Tillmann, R., Lee, B., Lopez-Hilfiker, F., Andres, S., Acir, I.-H., Rissanen, M.,  
660 Jokinen, T., Schobesberger, S., Kangasluoma, J., Kontkanen, J., Nieminen, T., Kurten, T.,  
661 Nielsen, L. B., Jorgensen, S., Kjaergaard, H. G., Canagaratna, M., Dal Maso, M., Berndt, T.,  
662 Petaja, T., Wahner, A., Kerminen, V.-M., Kulmala, M., Worsnop, D. R., Wildt, J., and Mentel,  
663 T. F.: A large source of low-volatility secondary organic aerosol, *Nature*, 506, 476, 2014.
- 664 Ervens, B., and Volkamer, R.: Glyoxal processing by aerosol multiphase chemistry:  
665 towards a kinetic modeling framework of secondary organic aerosol formation in  
666 aqueous particles, *Atmos. Chem. Phys.*, 10, 8219-8244, 2010.
- 667 Ervens, B., Turpin, B. J., and Weber, R. J.: Secondary organic aerosol formation in cloud  
668 droplets and aqueous particles (aqSOA): a review of laboratory, field and model studies,  
669 *Atmos. Chem. Phys.*, 11, 11069-11102, 2011.
- 670 Goldstein, A. H., and Galbally, I. E.: Known and unexplored organic constituents in the  
671 earth's atmosphere, *Environ. Sci. Technol.*, 41, 1514-1521, 2007.
- 672 Hallquist, M., Wenger, J. C., Baltensperger, U., Rudich, Y., Simpson, D., Claeys, M.,  
673 Dommen, J., Donahue, N. M., George, C., Goldstein, A. H., Hamilton, J. F., Herrmann, H.,  
674 Hoffmann, T., Iinuma, Y., Jang, M., Jenkin, M. E., Jimenez, J. L., Kiendler-Scharr, A.,  
675 Maenhaut, W., McFiggans, G., Mentel, T. F., Monod, A., Prevo, A. S. H., Seinfeld, J. H.,  
676 Surratt, J. D., Szmigielski, R., and Wildt, J.: The formation, properties and impact of  
677 secondary organic aerosol: current and emerging issues, *Atmos. Chem. Phys.*, 9, 5155-  
678 5235, 2009.
- 679 Hosny, N. A., Fitzgerald, C., Tong, C., Kalberer, M., Kuimova, M. K., and Pope, F. D.:  
680 Fluorescent lifetime imaging of atmospheric aerosols: a direct probe of aerosol viscosity,  
681 *Faraday Discuss.*, 165, 343-356, 2013.
- 682 Iinuma, Y., Boge, O., Gnauk, T., and Herrmann, H.: Aerosol-chamber study of the alpha-  
683 pinene/O<sub>3</sub> reaction: influence of particle acidity on aerosol yields and products, *Atmos.*  
684 *Environ.*, 38, 761-773, 2004.
- 685 Iinuma, Y., Muller, C., Berndt, T., Boge, O., Claeys, M., and Herrmann, H.: Evidence for the  
686 existence of organosulfates from beta-pinene ozonolysis in ambient secondary organic  
687 aerosol, *Environ. Sci. Technol.*, 41, 6678-6683, 2007.
- 688 Jang, M. S., Czoschke, N. M., Lee, S., and Kamens, R. M.: Heterogeneous atmospheric  
689 aerosol production by acid-catalyzed particle-phase reactions, *Science*, 298, 814-817,  
690 2002.
- 691 Jaoui, M., Corse, E., Kleindienst, T. E., Offenber, J. H., Lewandowski, M., and Edney, E. O.:  
692 Analysis of secondary organic aerosol compounds from the photooxidation of d-  
693 limonene in the presence of NO<sub>x</sub> and their detection in ambient PM<sub>2.5</sub>, *Environ. Sci.*  
694 *Technol.*, 40, 3819-3828, 2006.
- 695 Jimenez, J. L., Canagaratna, M. R., Donahue, N. M., Prevo, A. S. H., Zhang, Q., Kroll, J. H.,  
696 DeCarlo, P. F., Allan, J. D., Coe, H., Ng, N. L., Aiken, A. C., Docherty, K. S., Ulbrich, I. M.,

697 Grieshop, A. P., Robinson, A. L., Duplissy, J., Smith, J. D., Wilson, K. R., Lanz, V. A., Hueglin,  
698 C., Sun, Y. L., Tian, J., Laaksonen, A., Raatikainen, T., Rautiainen, J., Vaattovaara, P., Ehn,  
699 M., Kulmala, M., Tomlinson, J. M., Collins, D. R., Cubison, M. J., Dunlea, E. J., Huffman, J. A.,  
700 Onasch, T. B., Alfarra, M. R., Williams, P. I., Bower, K., Kondo, Y., Schneider, J., Drewnick,  
701 F., Borrmann, S., Weimer, S., Demerjian, K., Salcedo, D., Cottrell, L., Griffin, R., Takami, A.,  
702 Miyoshi, T., Hatakeyama, S., Shimono, A., Sun, J. Y., Zhang, Y. M., Dzepina, K., Kimmel, J. R.,  
703 Sueper, D., Jayne, J. T., Herndon, S. C., Trimborn, A. M., Williams, L. R., Wood, E. C.,  
704 Middlebrook, A. M., Kolb, C. E., Baltensperger, U., and Worsnop, D. R.: Evolution of  
705 organic aerosols in the atmosphere, *Science*, 326, 1525-1529, 2009.

706 Kahnt, A., Iinuma, Y., Blockhuys, F., Mutzel, A., Vermeylen, R., Kleindienst, T. E., Jaoui, M.,  
707 Offenberg, J. H., Lewandowski, M., Böge, O., Herrmann, H., Maenhaut, W., and Claeys, M.:  
708 2-Hydroxyterpenylic acid: An oxygenated marker compound for  $\alpha$ -pinene secondary  
709 organic aerosol in ambient fine aerosol, *Environ. Sci. Technol.*, 48, 4901-4908, 2014.

710 Kalberer, M., Sax, M., and Samburova, V.: Molecular size evolution of oligomers in  
711 organic aerosols collected in urban atmospheres and generated in a smog chamber,  
712 *Environ. Sci. Technol.*, 40, 5917-5922, 2006.

713 Kampf, C. J., Waxman, E. M., Slowik, J. G., Dommen, J., Pfaffenberger, L., Praplan, A. P.,  
714 Prevot, A. S. H., Baltensperger, U., Hoffmann, T., and Volkamer, R.: Effective Henry's Law  
715 Partitioning and the Salting Constant of Glyoxal in Aerosols Containing Sulfate, *Environ.*  
716 *Sci. Technol.*, 47, 4236-4244, 2013.

717 Kolb, C. E., Cox, R. A., Abbatt, J. P. D., Ammann, M., Davis, E. J., Donaldson, D. J., Garrett, B.  
718 C., George, C., Griffiths, P. T., Hanson, D. R., Kulmala, M., McFiggans, G., Pöschl, U.,  
719 Riipinen, I., Rossi, M. J., Rudich, Y., Wagner, P. E., Winkler, P. M., Worsnop, D. R., and O'  
720 Dowd, C. D.: An overview of current issues in the uptake of atmospheric trace gases by  
721 aerosols and clouds, *Atmos. Chem. Phys.*, 10, 10561-10605, 2010.

722 Koop, T., Bookhold, J., Shiraiwa, M., and Pöschl, U.: Glass transition and phase state of  
723 organic compounds: dependency on molecular properties and implications for  
724 secondary organic aerosols in the atmosphere, *Phys. Chem. Chem. Phys.*, 13, 19238-  
725 19255, 2011.

726 Kristensen, K., Cui, T., Zhang, H., Gold, A., Glasius, M., and Surratt, J. D.: Dimer esters in  $\alpha$ -  
727 pinene secondary organic aerosol: effect of hydroxyl radical, ozone, relative humidity  
728 and aerosol acidity, *Atmos. Chem. Phys.*, 14, 4201-4218, 2014.

729 Kroll, J. H., and Seinfeld, J. H.: Chemistry of secondary organic aerosol: Formation and  
730 evolution of low-volatility organics in the atmosphere, *Atmos. Environ.*, 42, 3593-3624,  
731 2008.

732 Kundu, S., Fisseha, R., Putman, A. L., Rahn, T. A., and Mazzoleni, L. R.: High molecular  
733 weight SOA formation during limonene ozonolysis: insights from ultrahigh-resolution  
734 FT-ICR mass spectrometry characterization, *Atmos. Chem. Phys.*, 12, 5523-5536, 2012.

735 Kuwata, M., and Martin, S. T.: Phase of atmospheric secondary organic material affects  
736 its reactivity, *Proc Natl Acad Sci USA*, 109, 17354-17359, 2012.

737 Laskin, A., Laskin, J., and Nizkorodov, S. A.: Mass spectrometric approaches for chemical  
738 characterisation of atmospheric aerosols: critical review of the most recent advances,  
739 *Environ. Chem.*, 9, 163-189, 2012a.

- 740 Laskin, J., Eckert, P. A., Roach, P. J., Heath, B. S., Nizkorodov, S. A., and Laskin, A.: Chemical  
741 Analysis of Complex Organic Mixtures Using Reactive Nanospray Desorption  
742 Electrospray Ionization Mass Spectrometry, *Anal. Chem.*, 84, 7179-7187, 2012b.
- 743 Liggio, J., Li, S. M., and McLaren, R.: Heterogeneous reactions of glyoxal on particulate  
744 matter: Identification of acetals and sulfate esters, *Environ. Sci. Technol.*, 39, 1532-1541,  
745 2005.
- 746 Lim, Y. B., Tan, Y., Perri, M. J., Seitzinger, S. P., and Turpin, B. J.: Aqueous chemistry and its  
747 role in secondary organic aerosol (SOA) formation, *Atmos. Chem. Phys.*, 10, 10521-  
748 10539, 2010.
- 749 Lin, Y.-H., Zhang, Z., Docherty, K. S., Zhang, H., Budisulistiorini, S. H., Rubitschun, C. L.,  
750 Shaw, S. L., Knipping, E. M., Edgerton, E. S., Kleindienst, T. E., Gold, A., and Surratt, J. D.:  
751 Isoprene Epoxydiols as Precursors to Secondary Organic Aerosol Formation: Acid-  
752 Catalyzed Reactive Uptake Studies with Authentic Compounds, *Environ. Sci. Technol.*,  
753 46, 250-258, 2012.
- 754 Lin, Y.-H., Zhang, H., Pye, H. O. T., Zhang, Z., Marth, W. J., Park, S., Arashiro, M., Cui, T.,  
755 Budisulistiorini, S. H., Sexton, K. G., Vizuete, W., Xie, Y., Luecken, D. J., Piletic, I. R., Edney,  
756 E. O., Bartolotti, L. J., Gold, A., and Surratt, J. D.: Epoxide as a precursor to secondary  
757 organic aerosol formation from isoprene photooxidation in the presence of nitrogen  
758 oxides, *Proc Natl Acad Sci USA*, 110, 6718-6723, 2013.
- 759 Loza, C. L., Craven, J. S., Yee, L. D., Coggon, M. M., Schwantes, R. H., Shiraiwa, M., Zhang, X.,  
760 Schilling, K. A., Ng, N. L., Canagaratna, M. R., Ziemann, P. J., Flagan, R. C., and Seinfeld, J. H.:  
761 Secondary organic aerosol yields of 12-carbon alkanes, *Atmos. Chem. Phys.*, 14, 1423-  
762 1439, 2014.
- 763 McNeill, V. F., Woo, J. L., Kim, D. D., Schwier, A. N., Wannell, N. J., Sumner, A. J., and  
764 Barakat, J. M.: Aqueous-phase secondary organic aerosol and organosulfate formation in  
765 atmospheric aerosols: A modeling study, *Environ. Sci. Technol.*, 46, 8075-8081, 2012.
- 766 Murphy, B. N., Donahue, N. M., Robinson, A. L., and Pandis, S. N.: A naming convention for  
767 atmospheric organic aerosol, *Atmos. Chem. Phys.*, 14, 5825-5839, 2014.
- 768 Nguyen, T. B., Laskin, J., Laskin, A., and Nizkorodov, S. A.: Nitrogen-Containing Organic  
769 Compounds and Oligomers in Secondary Organic Aerosol Formed by Photooxidation of  
770 Isoprene, *Environ. Sci. Technol.*, 45, 6908-6918, 2011.
- 771 Nguyen, T. B., Nizkorodov, S. A., Laskin, A., and Laskin, J.: An approach toward  
772 quantification of organic compounds in complex environmental samples using high-  
773 resolution electrospray ionization mass spectrometry, *Analytical Methods*, 5, 72-80,  
774 2013.
- 775 Offenberg, J. H., Lewandowski, M., Edney, E. O., Kleindienst, T. E., and Jaoui, M.: Influence  
776 of Aerosol Acidity on the Formation of Secondary Organic Aerosol from Biogenic  
777 Precursor Hydrocarbons, *Environ. Sci. Technol.*, 43, 7742-7747, 2009.
- 778 Pankow, J. F.: An absorption-model of the gas aerosol partitioning involved in the  
779 formation of secondary organic aerosol, *Atmos. Environ.*, 28, 189-193, 1994.
- 780 Perraud, V., Bruns, E. A., Ezell, M. J., Johnson, S. N., Yu, Y., Alexander, M. L., Zelenyuk, A.,  
781 Imre, D., Chang, W. L., Dabdub, D., Pankow, J. F., and Finlayson-Pitts, B. J.:

- 782 Nonequilibrium atmospheric secondary organic aerosol formation and growth, Proc  
783 Natl Acad Sci USA, 109, 2836-2841, 2012.
- 784 Pfrang, C., Shiraiwa, M., and Pöschl, U.: Chemical ageing and transformation of diffusivity  
785 in semi-solid multi-component organic aerosol particles, Atmos. Chem. Phys., 11, 7343-  
786 7354, 2011.
- 787 Pierce, J. R., Riipinen, I., Kulmala, M., Ehn, M., Petäjä, T., Junninen, H., Worsnop, D. R., and  
788 Donahue, N. M.: Quantification of the volatility of secondary organic compounds in  
789 ultrafine particles during nucleation events, Atmos. Chem. Phys., 11, 9019-9036, 2011.
- 790 Pöschl, U., Rudich, Y., and Ammann, M.: Kinetic model framework for aerosol and cloud  
791 surface chemistry and gas-particle interactions - Part 1: General equations, parameters,  
792 and terminology, Atmos. Chem. Phys., 7, 5989-6023, 2007.
- 793 Presto, A. A., Hartz, K. E. H., and Donahue, N. M.: Secondary organic aerosol production  
794 from terpene ozonolysis. 2. Effect of NO<sub>x</sub> concentration, Environ. Sci. Technol., 39, 7046-  
795 7054, 2005.
- 796 Renbaum-Wolff, L., Grayson, J. W., Bateman, A. P., Kuwata, K., Sellier, M., Murray, B. J.,  
797 Schilling, J. E., Martin, S. T., and Bertram, A. K.: Viscosity of  $\alpha$ -pinene secondary organic  
798 material and implications for particle growth and reactivity, Proc Natl Acad Sci USA,  
799 110, 8014-8019, 2013.
- 800 Riipinen, I., Pierce, J. R., Yli-Juuti, T., Nieminen, T., Hakkinen, S., Ehn, M., Junninen, H.,  
801 Lehtipalo, K., Petaja, T., Slowik, J., Chang, R., Shantz, N. C., Abbatt, J., Leaitch, W. R.,  
802 Kerminen, V. M., Worsnop, D. R., Pandis, S. N., Donahue, N. M., and Kulmala, M.: Organic  
803 condensation: a vital link connecting aerosol formation to cloud condensation nuclei  
804 (CCN) concentrations, Atmos. Chem. Phys., 11, 3865-3878, 2011.
- 805 Sareen, N., Schwier, A. N., Shapiro, E. L., Mitroo, D., and McNeill, V. F.: Secondary organic  
806 material formed by methylglyoxal in aqueous aerosol mimics, Atmos. Chem. Phys., 10,  
807 997-1016, 2010.
- 808 Schilling-Fahnestock, K. A., Yee, L. D., Loza, C. L., Coggon, M. M., Schwantes, R., Zhang, X.,  
809 Dalleska, N. F., and Seinfeld, J. H.: Secondary Organic Aerosol Composition from C12  
810 Alkanes, J. Phys. Chem. A, doi: 10.1021/jp501779w, 2014.
- 811 Schobesberger, S., Junninen, H., Bianchi, F., Lonn, G., Ehn, M., Lehtipalo, K., Dommen, J.,  
812 Ehrhart, S., Ortega, I. K., Franchin, A., Nieminen, T., Riccobono, F., Hutterli, M., Duplissy, J.,  
813 Almeida, J., Amorim, A., Breitenlechner, M., Downard, A. J., Dunne, E. M., Flagan, R. C.,  
814 Kajos, M., Keskinen, H., Kirkby, J., Kupc, A., Kuerten, A., Kurten, T., Laaksonen, A., Mathot,  
815 S., Onnela, A., Praplan, A. P., Rondo, L., Santos, F. D., Schallhart, S., Schnitzhofer, R., Sipila,  
816 M., Tome, A., Tsagkogeorgas, G., Vehkamäki, H., Wimmer, D., Baltensperger, U., Carslaw,  
817 K. S., Curtius, J., Hansel, A., Petaja, T., Kulmala, M., Donahue, N. M., and Worsnop, D. R.:  
818 Molecular understanding of atmospheric particle formation from sulfuric acid and large  
819 oxidized organic molecules, Proc Natl Acad Sci USA, 110, 17223-17228, 2013.
- 820 Shiraiwa, M., Ammann, M., Koop, T., and Pöschl, U.: Gas uptake and chemical aging of  
821 semisolid organic aerosol particles, Proc Natl Acad Sci USA, 108, 11003-11008, 2011.
- 822 Shiraiwa, M., Pfrang, C., Koop, T., and Pöschl, U.: Kinetic multi-layer model of gas-particle  
823 interactions in aerosols and clouds (KM-GAP): linking condensation, evaporation and



- 824 chemical reactions of organics, oxidants and water, *Atmos. Chem. Phys.*, 12, 2777-2794,  
825 2012.
- 826 Shiraiwa, M., and Seinfeld, J. H.: Equilibration timescale of atmospheric secondary  
827 organic aerosol partitioning, *Geophys. Res. Lett.*, 39, L24801, 2012.
- 828 Shiraiwa, M., Yee, L. D., Schilling, K. A., Loza, C. L., Craven, J. S., Zuend, A., Ziemann, P. J.,  
829 and Seinfeld, J. H.: Size distribution dynamics reveal particle-phase chemistry in organic  
830 aerosol formation, *Proc Natl Acad Sci USA*, 110, 11746-11750, 2013a.
- 831 Shiraiwa, M., Zuend, A., Bertram, A. K., and Seinfeld, J. H.: Gas-particle partitioning of  
832 atmospheric aerosols: interplay of physical state, non-ideal mixing and morphology,  
833 *Phys. Chem. Chem. Phys.*, 15, 11441-11453, 2013b.
- 834 Surratt, J. D., Murphy, S. M., Kroll, J. H., Ng, N. L., Hildebrandt, L., Sorooshian, A.,  
835 Szmigielski, R., Vermeylen, R., Maenhaut, W., Claeys, M., Flagan, R. C., and Seinfeld, J. H.:  
836 Chemical composition of secondary organic aerosol formed from the photooxidation of  
837 isoprene, *J. Phys. Chem. A*, 110, 9665-9690, 2006.
- 838 Surratt, J. D., Gomez-Gonzalez, Y., Chan, A. W. H., Vermeylen, R., Shahgholi, M.,  
839 Kleindienst, T. E., Edney, E. O., Offenberg, J. H., Lewandowski, M., Jaoui, M., Maenhaut, W.,  
840 Claeys, M., Flagan, R. C., and Seinfeld, J. H.: Organosulfate formation in biogenic  
841 secondary organic aerosol, *J. Phys. Chem. A*, 112, 8345-8378, 2008.
- 842 Surratt, J. D., Chan, A. W. H., Eddingsaas, N. C., Chan, M. N., Loza, C. L., Kwan, A. J., Hersey,  
843 S. P., Flagan, R. C., Wennberg, P. O., and Seinfeld, J. H.: Reactive intermediates revealed in  
844 secondary organic aerosol formation from isoprene, *Proc Natl Acad Sci USA*, 107, 6640-  
845 6645, 2010.
- 846 Trump, E. R., and Donahue, N. M.: Oligomer formation within secondary organic  
847 aerosols: equilibrium and dynamic considerations, *Atmos. Chem. Phys.*, 14, 3691-3701,  
848 2014.
- 849 Vaden, T. D., Imre, D., Beranek, J., Shrivastava, M., and Zelenyuk, A.: Evaporation kinetics  
850 and phase of laboratory and ambient secondary organic aerosol, *Proc Natl Acad Sci USA*,  
851 108, 2190-2195, 2011.
- 852 Virtanen, A., Joutsensaari, J., Koop, T., Kannosto, J., YliPirilä, P., Leskinen, J., Mäkelä, J. M.,  
853 Holopainen, J. K., Pöschl, U., Kulmala, M., Worsnop, D. R., and Laaksonen, A.: An  
854 amorphous solid state of biogenic secondary organic aerosol particles, *Nature*, 467, 824-  
855 827, 2010.
- 856 Vogel, A. L., Äijälä, M., Corrigan, A. L., Junninen, H., Ehn, M., Petäjä, T., Worsnop, D. R.,  
857 Kulmala, M., Russell, L. M., Williams, J., and Hoffmann, T.: In situ submicron organic  
858 aerosol characterization at a boreal forest research station during HUMPPA-COPEC  
859 2010 using soft and hard ionization mass spectrometry, *Atmos. Chem. Phys.*, 13, 10933-  
860 10950, 2013.
- 861 Williams, B. J., Goldstein, A. H., Kreisberg, N. M., and Hering, S. V.: In situ measurements  
862 of gas/particle-phase transitions for atmospheric semivolatile organic compounds, *Proc  
863 Natl Acad Sci USA*, 107, 6676-6681, 2010.
- 864 Worsnop, D. R., Morris, J. W., Shi, Q., Davidovits, P., and Kolb, C. E.: A chemical kinetic  
865 model for reactive transformations of aerosol particles, *Geophys. Res. Lett.*, 29, 57, 2002.

866 Xu, L., Kollman, M. S., Song, C., Shilling, J. E., and Ng, N. L.: Effects of NO<sub>x</sub> on the Volatility  
867 of Secondary Organic Aerosol from Isoprene Photooxidation, *Environ. Sci. Technol.*, 48,  
868 2253-2262, 2014.

869 Yee, L. D., Craven, J. S., Loza, C. L., Schilling, K. A., Ng, N. L., Canagaratna, M. R., Ziemann, P.  
870 J., Flagan, R. C., and Seinfeld, J. H.: Secondary organic aerosol formation from low-NO<sub>x</sub>  
871 photooxidation of dodecane: evolution of multigeneration gas-phase chemistry and  
872 aerosol composition, *J. Phys. Chem. A*, 116, 6211-6230, 2012.

873 Zaveri, R. A., Easter, R. C., Shilling, J. E., and Seinfeld, J. H.: Modeling kinetic partitioning of  
874 secondary organic aerosol and size distribution dynamics: representing effects of  
875 volatility, phase state, and particle-phase reaction, *Atmos. Chem. Phys.*, 14, 5153-5181,  
876 2014.

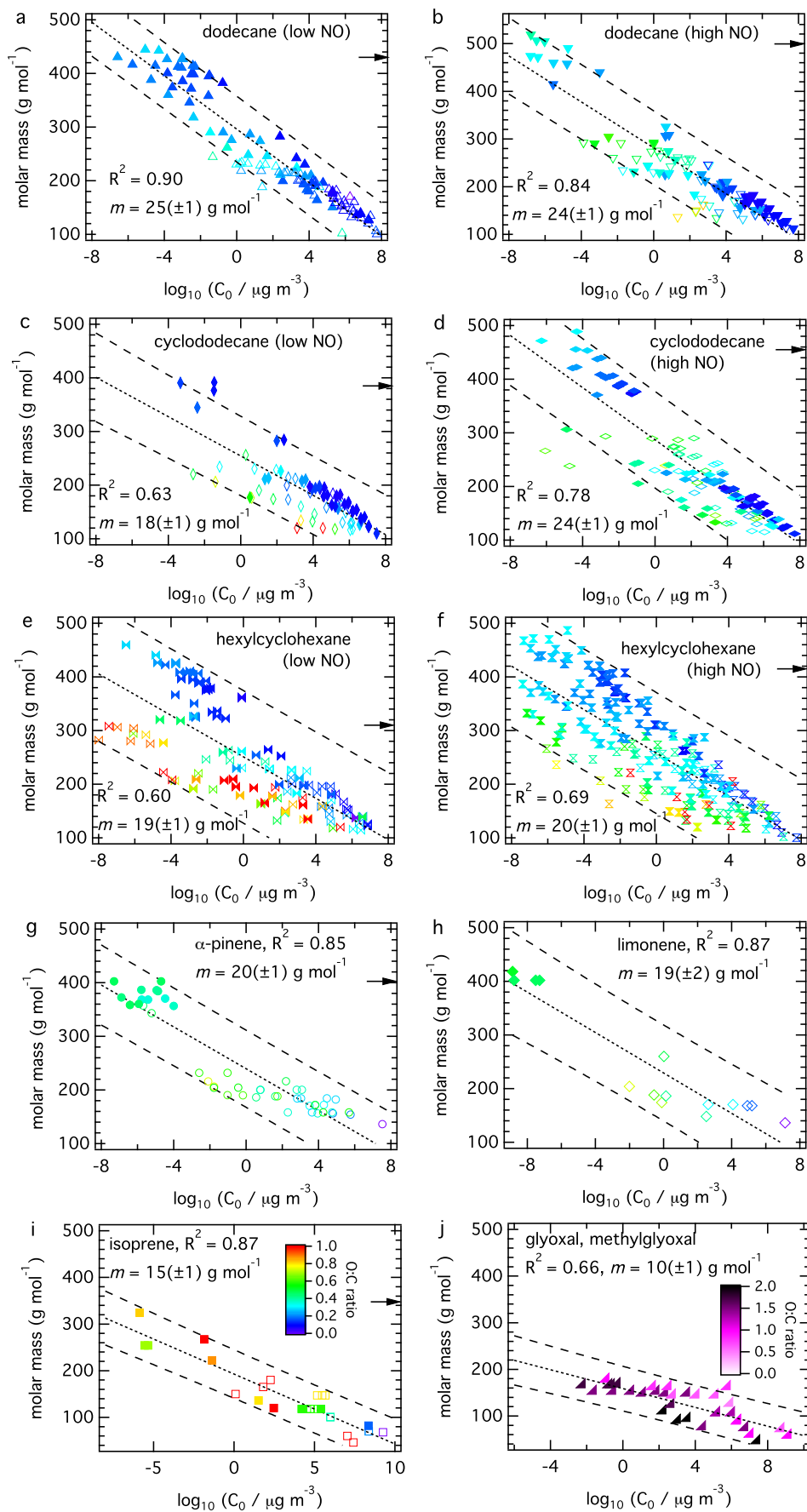
877 Zhang, X., Pandis, S. N., and Seinfeld, J. H.: Diffusion-limited versus quasi-equilibrium  
878 aerosol growth, *Aerosol Sci. Technol.*, 46, 874-885, 2012.

879 Zhao, R., Lee, A. K. Y., and Abbatt, J. P. D.: Investigation of Aqueous-Phase Photooxidation  
880 of Glyoxal and Methylglyoxal by Aerosol Chemical Ionization Mass Spectrometry:  
881 Observation of Hydroxyhydroperoxide Formation, *J. Phys. Chem. A*, 116, 6253-6263,  
882 2012.

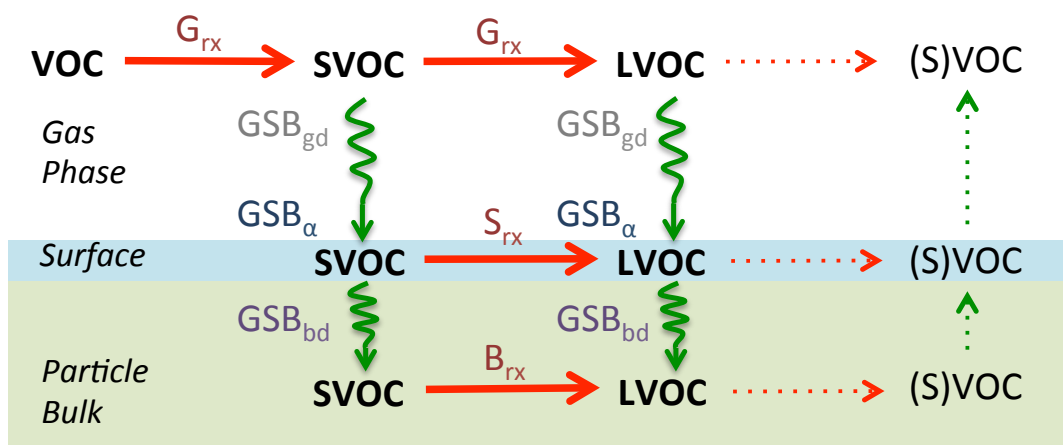
883 Zhou, S., Shiraiwa, M., McWhinney, R., Pöschl, U., and Abbatt, J. P. D.: Kinetic limitations  
884 in gas-particle reactions arising from slow diffusion in secondary organic aerosol,  
885 *Faraday Discuss.*, 165, 391-406, 2013.

886 Ziemann, P. J., and Atkinson, R.: Kinetics, products, and mechanisms of secondary  
887 organic aerosol formation, *Chem. Soc. Rev.*, 41, 6582-6605, 2012.

888 Zuend, A., and Seinfeld, J. H.: Modeling the gas-particle partitioning of secondary organic  
889 aerosol: the importance of liquid-liquid phase separation, *Atmos. Chem. Phys.*, 12, 3857-  
890 3882, 2012.  
891  
892

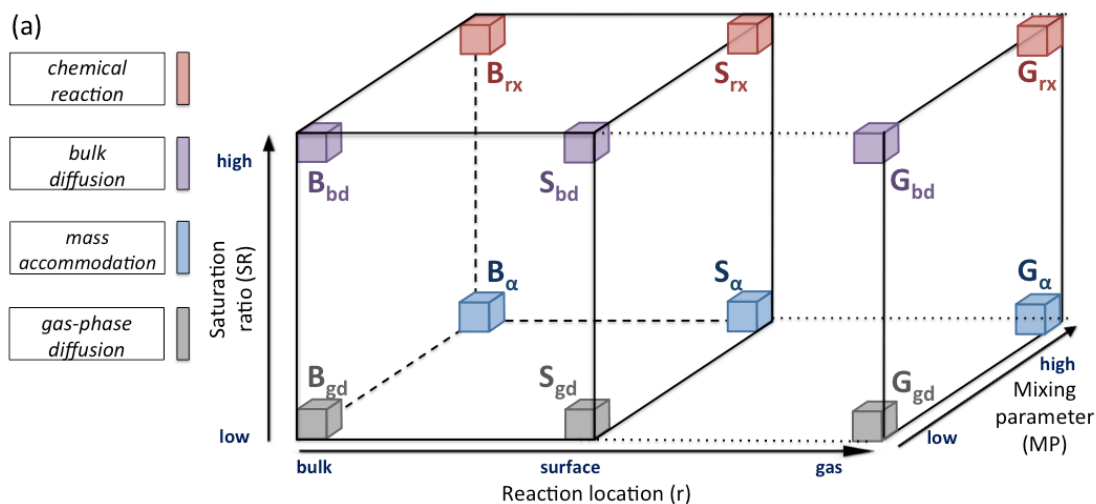


894 **Figure 1.** Molecular corridors of SOA evolution for different precursor compounds.  
895 Molar mass vs. volatility (saturation mass concentration,  $C_0$ ) at 298 K for oxidation  
896 products of dodecane at low (a) and high (b) NO condition, cyclododecane at low (c)  
897 and high (d) NO condition, and hexylcyclohexane at low (e) and high (f) NO  
898 condition and isoprene (g),  $\alpha$ -pinene (h), limonene (i), and glyoxal and methylglyoxal  
899 (j). The open and solid markers correspond to the gas- and particle-phase products,  
900 respectively, color-coded by atomic O:C ratio (note different color scale for panel j).  
901 With a linear regression analysis, the coefficient of determination ( $R^2$ ), fitted lines  
902 (dotted lines) and their slopes ( $m$ ), and prediction intervals with 95% confidence  
903 (dashed lines) are shown. The arrows on the right axis indicate average molar mass  
904 for isoprene and  $\alpha$ -pinene (Kalberer et al., 2006) as well as for alkanes as measured in  
905 this study.  
906

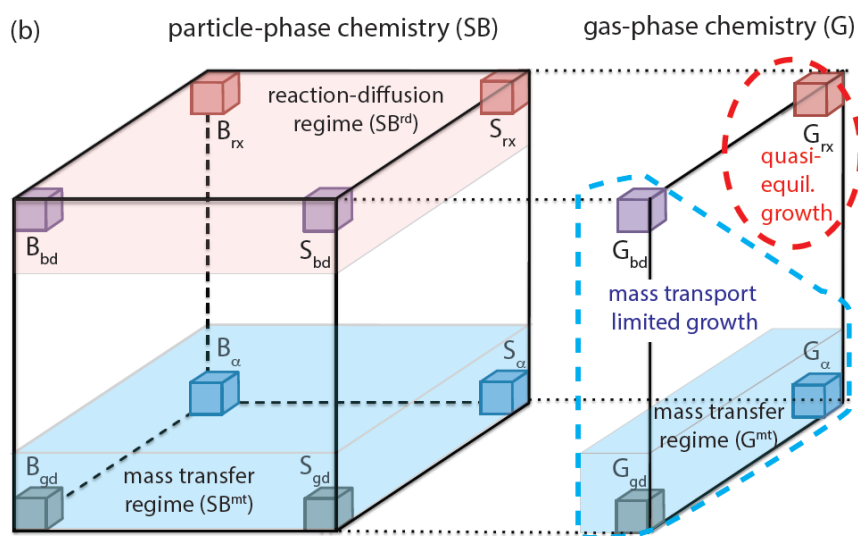


907

908 **Figure 2.** Molecular processes of SOA evolution: schematic outline of formation and  
 909 aging. Red and green arrows denote chemical reactions and mass transport,  
 910 respectively. Sequential and parallel reactions in the gas phase, at the particle surface,  
 911 and in the particle bulk lead to multiple generations of volatile, semi-volatile and low-  
 912 volatile organic compounds (VOC, SVOC, LVOC). Dotted arrows denote  
 913 revolatilization resulting from fragmentation reactions. Labels on arrows relate to  
 914 kinetic regimes outlined in subsequent figure.

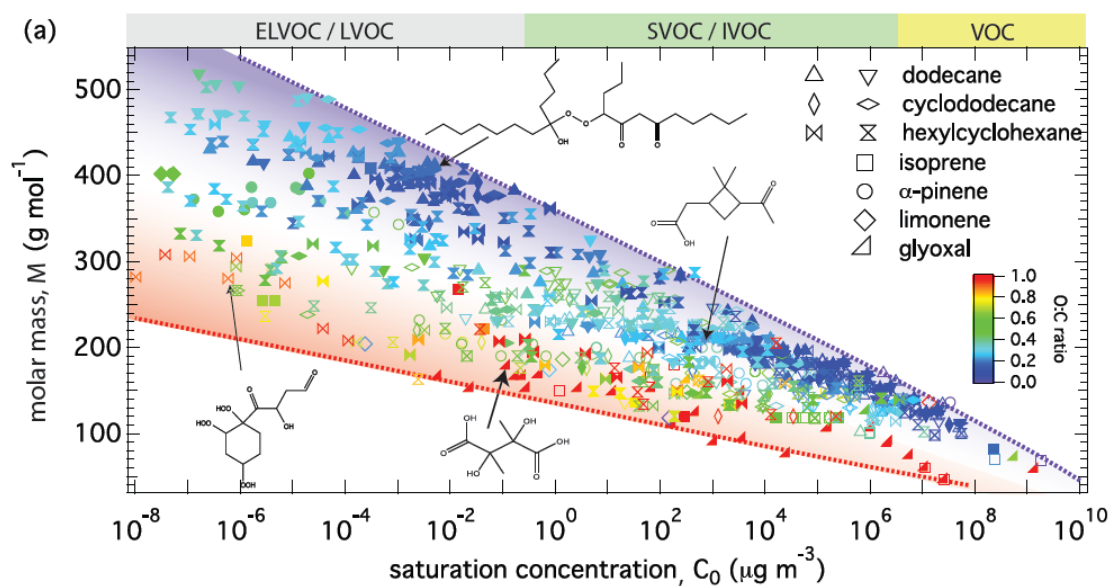


915

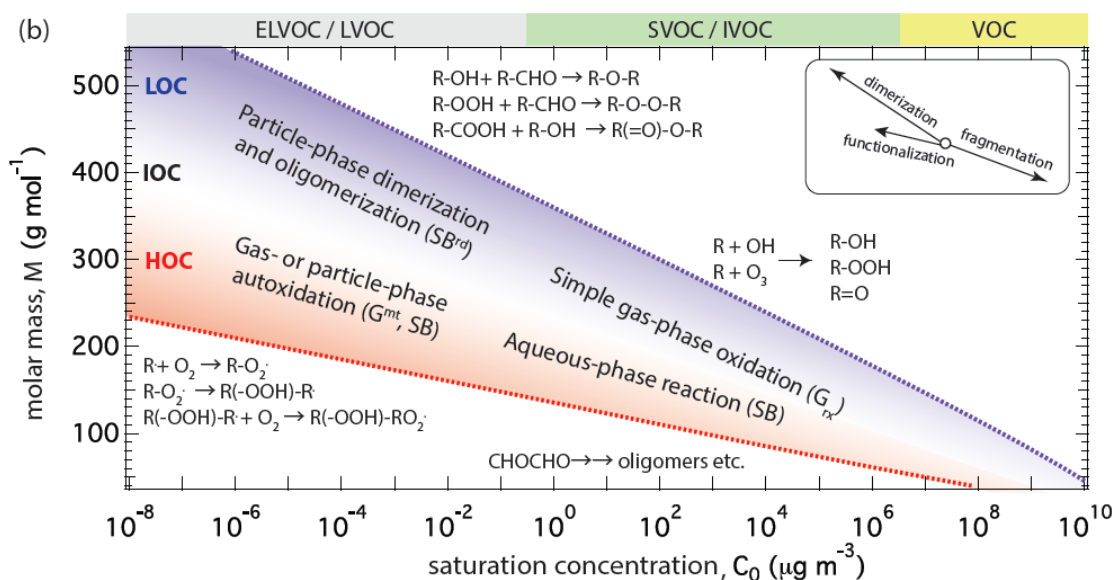


916

917 **Figure 3.** Kinetic regimes and limiting cases of SOA evolution mapped onto the axes  
 918 of a cuboid representing reaction location, saturation ratio, and mixing parameter. (a)  
 919 Horizontal edges of the cuboid (left to right) correspond to four regimes governed by  
 920 chemical reaction (“rx”, red), bulk diffusion (“bd”, purple), mass accommodation (“  
 921  $\alpha$ ”, blue), or gas-phase diffusion (“gd”, grey). Each of these regimes includes three  
 922 distinct limiting cases characterized by a single rate-limiting process and a dominant  
 923 reaction location (particle bulk, B; surface, S; gas phase, G). (b) The left side of the  
 924 cuboid can be regarded as a particle-phase chemistry regime (SB) and subdivided into  
 925 a reaction-diffusion regime ( $SB^{rd}$ ) and a mass transfer regime ( $SB^{mt}$ ). The right side of  
 926 the cuboid can be regarded as a gas-phase chemistry regime (G) and subdivided into a  
 927 traditional scenario of “quasi-equilibrium growth” limited only by a gas phase  
 928 reaction followed by quasi-instantaneous gas-particle partitioning ( $G_{rx}$ ) and a mass-  
 929 transport limited regime of “non-equilibrium growth” that may be kinetically limited  
 930 by gas-to-particle mass transfer ( $G^{mt}$ ) or diffusion in the particle ( $G_{bd}$ ).



931



932

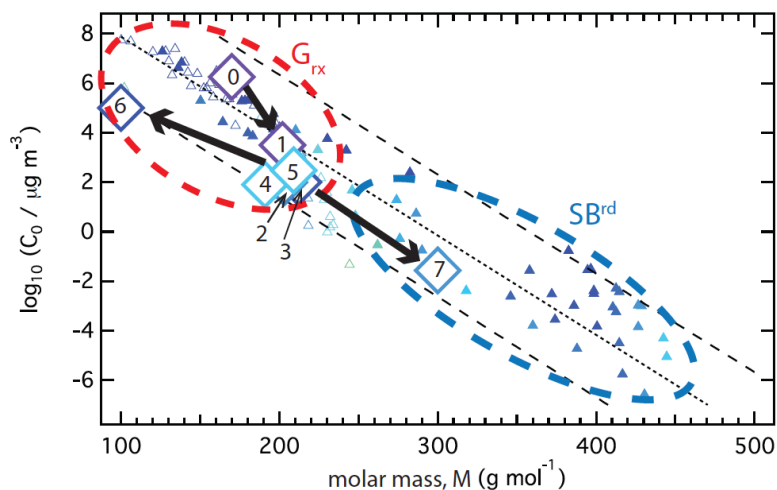
933 **Figure 4.** Ensemble of molecular corridors and kinetic regimes of SOA evolution. (a)  
 934 Molar mass vs. volatility ( $C_0$ ) at 298 K for gas-phase (open) and particle-phase (solid)  
 935 oxidation products of anthropogenic precursors (dodecane, cyclododecane,  
 936 hexylcyclohexane) under low/high NO conditions, biogenic precursors ( $\alpha$ -pinene,  
 937 limonene, isoprene) and aqueous-phase reaction products of glyoxal and  
 938 methylglyoxal. The dotted lines represent linear alkanes  $C_nH_{2n+2}$  (purple with O:C =  
 939 0) and sugar alcohols  $C_nH_{2n+2}O_n$  (red with O:C = 1). Chemical structures of some  
 940 representative products are shown. (b) Characteristic reaction pathways with most  
 941 probable kinetic regimes. Molecular corridors consists of high, intermediate and low  
 942 O:C corridors (HOC, red shaded area; IOC, white area; LOC, blue shaded area). SOA  
 943 products evolve over the molecular corridor driven by three key reaction types of

944 functionalization, oligomerization and fragmentation as illustrated in the insert (note  
945 different lengths of arrows indicating different intensities of effects on volatility).

946

947

948



949

950 **Figure 5.** Evolution of reaction pathways over the molecular corridor of dodecane  
951 SOA under low NO condition. The large diamonds indicate the surrogate compounds  
952 used in the KM-GAP simulations (Appendix D; Shiraiwa et al., 2013a), including the  
953 precursor (dodecane, 0), 1<sup>st</sup> – 5th generations of surrogate products of gas-phase  
954 oxidation (1-5), gas-phase fragmentation (aldehydes, 6), and particle-phase  
955 dimerization products (7). The smaller symbols indicate identified individual products  
956 (as shown in Fig. 1a).

957

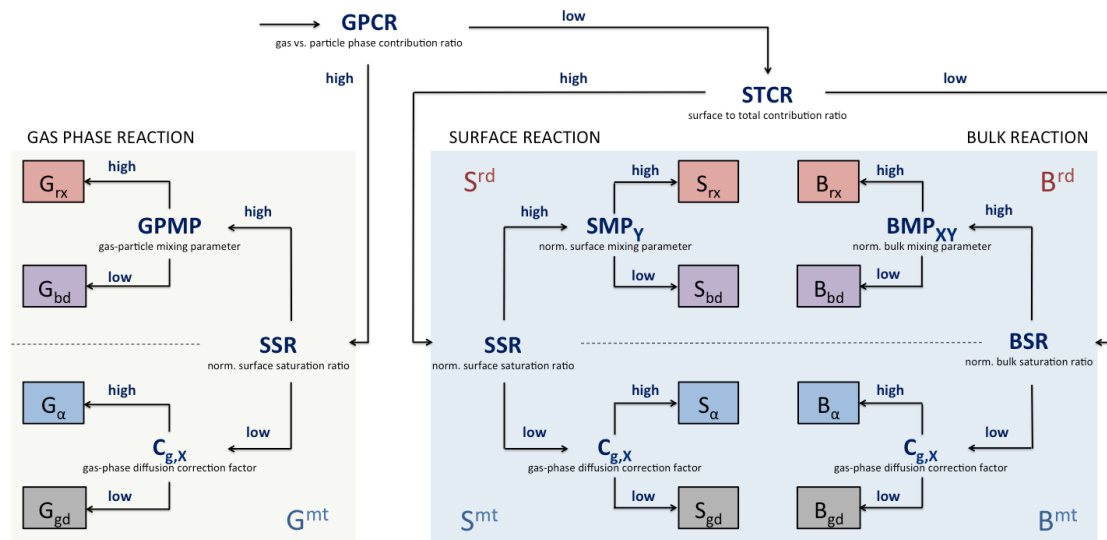


958 **Table 1.** Summary of analysis of identified SOA oxidation products. Number of  
 959 identified oxidation products  $N$ , average molar mass  $M_{\text{ave}}$ , negative slope ( $-$   
 960  $dM/d\log C_0$ ) of fitted lines in Fig. 2 of molar mass vs. logarithm of volatility,  
 961 coefficients of determination  $R^2$  as well as  $R^2$  for O:C vs. logarithm of volatility

precursor	$N$	$M_{\text{ave}}$ (g mol <sup>-1</sup> )	$-dM/d\log C_0$ (g mol <sup>-1</sup> )	$R^2$ (molar mass)	$R^2$ (O:C)
dodecane, low NO	116	429	25(±1)	0.90	0.22
dodecane, high NO	106	495	24(±1)	0.84	0.29
cyclododecane, low NO	77	384	18(±1)	0.63	0.08
cyclododecane, high NO	122	458	24(±1)	0.78	0.08
hexylcyclohexane, low NO	137	310	19(±1)	0.60	0.05
hexylcyclohexane, high NO	230	418	20(±1)	0.69	0.00
α-pinene	47	400*	20(±1)	0.85	0.13
limonene	17	-	19(±2)	0.87	0.38
isoprene	29	350*	15(±1)	0.87	0.09
glyoxal, methylglyoxal	35	-	10(±1)	0.66	0.16

962 \* (Kalberer et al., 2006)

963

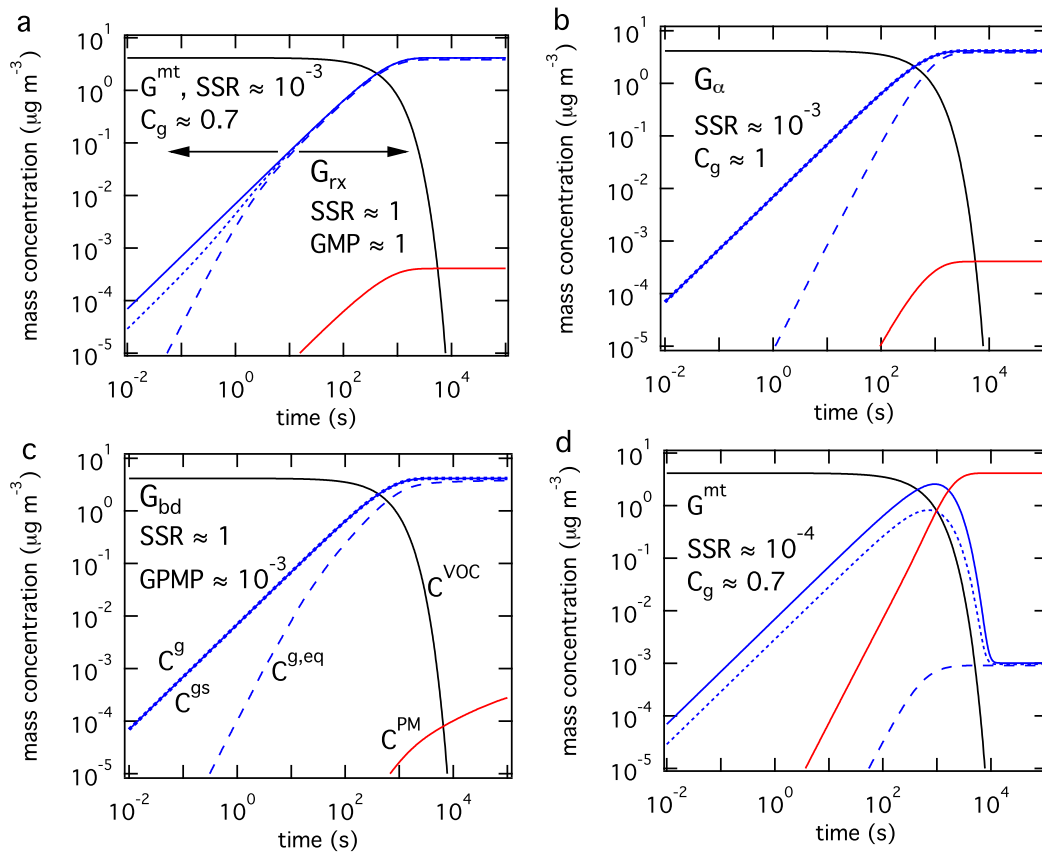


964

**GAS-PHASE REGIME**

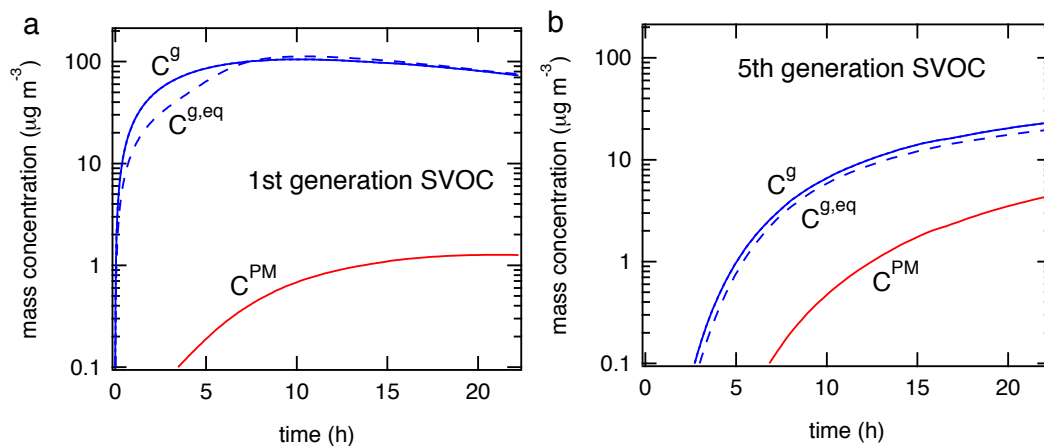
**PARTICLE-PHASE REGIME**

965 **Figure A1.** Decision tree for classification and distinction of limiting cases for  
 966 multiphase chemical evolution of SOA. The classification is based on: 1) the location  
 967 of the reaction leading to its formation, 2) its saturation ratio, and 3) its mixing  
 968 parameter to assess the heterogeneity in the gas and particle phases. The resulting  
 969 limiting cases are shown in the small boxes with reaction location in the gas phase  
 970 (G), at the surface (S) and in the bulk (B) and limiting processes of chemical reaction  
 971 (rx), bulk diffusion (bd), mass accommodation ( $\alpha$ ), and gas-phase diffusion (gd).

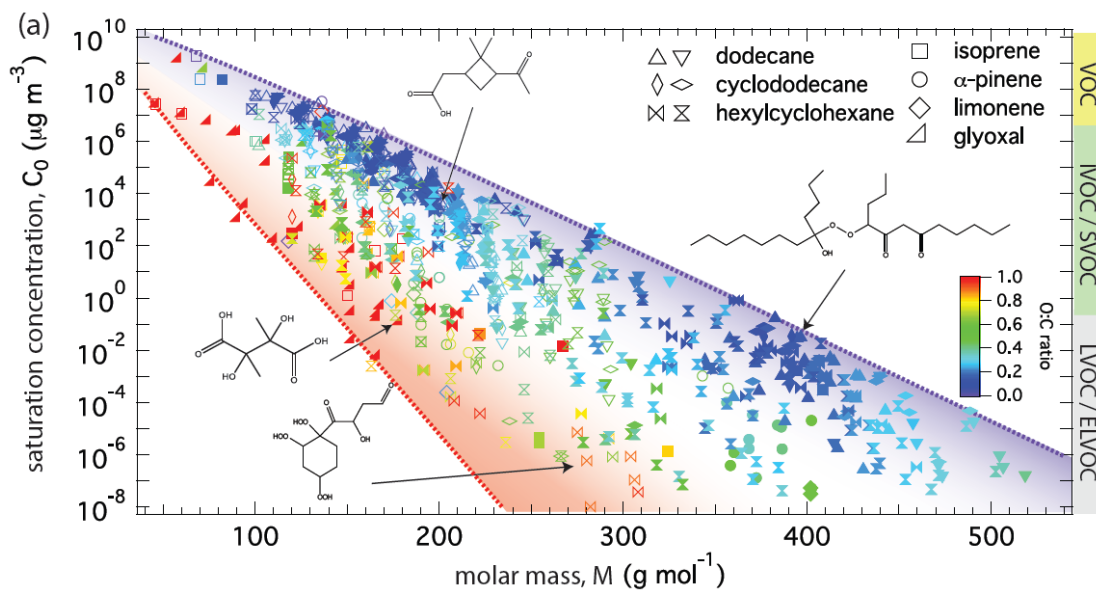


972

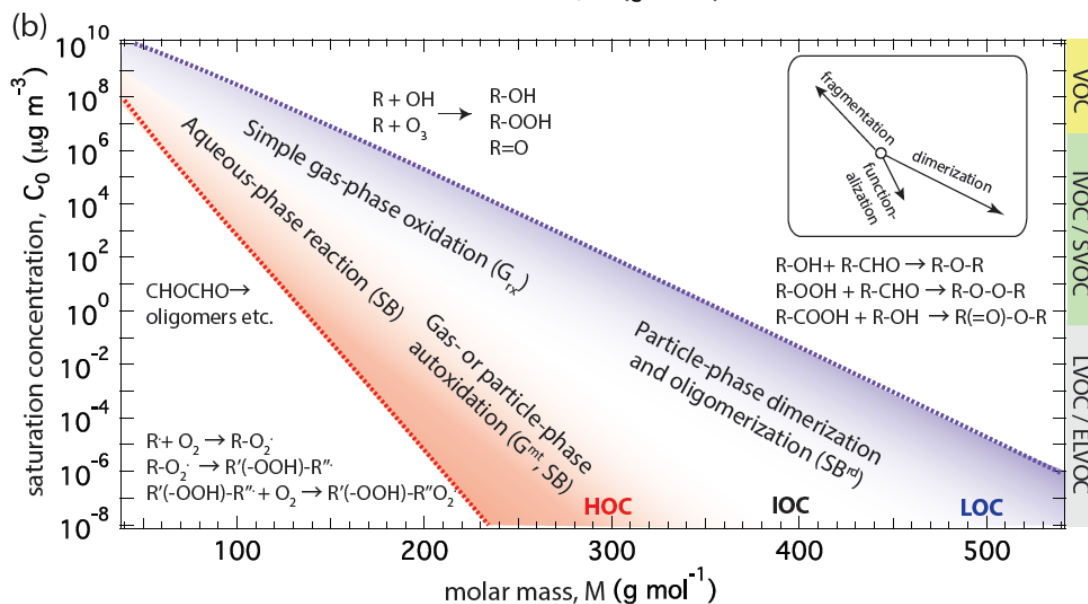
973 **Figure A2.** Temporal evolution of mass concentration of the hypothesized VOC  
 974 oxidation product in the gas phase (solid blue), in the near-surface gas phase (dotted  
 975 blue), in the particle phase (red), and equilibrium gas-phase concentration (dashed  
 976 blue). The gas-phase mass concentration of the parent VOC is shown by the black  
 977 line. For semi-volatile oxidation products with  $C^* = 10^3 \mu\text{g m}^{-3}$ , SOA growth is  
 978 limited by (a) gas-phase reaction ( $G_{rx}$ ), (b) accommodation ( $G_\alpha$ ), and (c) bulk  
 979 diffusion ( $G_{bd}$ ). Panel (d) shows an exemplary simulation for LVOCs with  $C^* = 10^3$   
 980  $\mu\text{g m}^{-3}$  exhibiting kinetic limitation in the gas-particle mass transfer regime ( $G^{mt}$ ).  
 981



982  
 983 **Figure A3.** Modeling SOA formation from dodecane photooxidation. Temporal  
 984 evolution of mass concentration of the (a) 1<sup>st</sup> and (b) 5th generation products in the  
 985 gas (solid blue) and particle phases (red) and equilibrium gas-phase mass  
 986 concentration (dashed blue).



987



988

989 **Figure A4.** Alternative representation of molecular corridors (Fig. 4) displaying  
 990 volatility ( $C_0$ ) as a function of molar mass, which appears more straightforward to use  
 991 and interpret in mechanistic studies (see Fig. 5) and for direct comparison to mass  
 992 spectra. Volatility decreases as molar mass increases from left to right, and the slope  
 993  $d\log C_0/dM$  is steeper for molecules with higher O:C ratio and polarity due to stronger  
 994 hydrogen bonding and evaporation enthalpy.

995

996 **Table A1.** Experimental conditions in studies identifying oxidation products as  
 997 included in Figures 1 and 4.

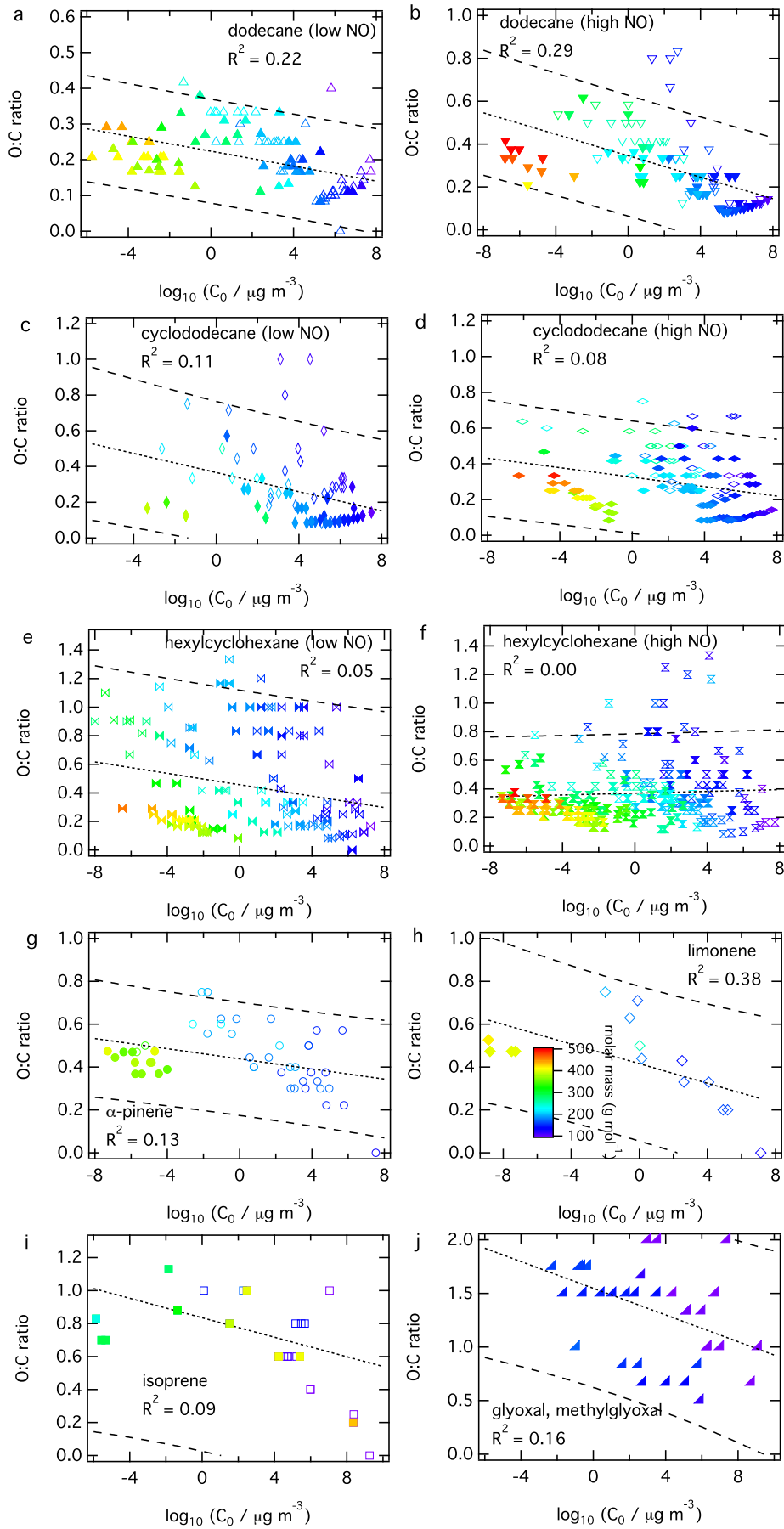
	study	oxidants	NO	seed
dodecane		OH	low / high	(NH <sub>4</sub> ) <sub>2</sub> SO <sub>4</sub>
cyclododecane	this study, Schilling-Fahnestock et al., 2014	OH	low / high	(NH <sub>4</sub> ) <sub>2</sub> SO <sub>4</sub>
hexylcyclohexane		OH	low / high	(NH <sub>4</sub> ) <sub>2</sub> SO <sub>4</sub>
α-pinene	Docherty et al 2005	O <sub>3</sub>	low	no seed
	Claeys et al., 2007	OH	high	no seed
	Claeys et al., 2009	OH, O <sub>3</sub>	high / low	(NH <sub>4</sub> ) <sub>2</sub> SO <sub>4</sub> , H <sub>2</sub> SO <sub>4</sub> , MgSO <sub>4</sub>
	Kahnt et al., 2014	O <sub>3</sub>	high	(NH <sub>4</sub> ) <sub>2</sub> SO <sub>4</sub> , H <sub>2</sub> SO <sub>4</sub>
	Kristensen et al., 2014	OH, O <sub>3</sub>	high	(NH <sub>4</sub> ) <sub>2</sub> SO <sub>4</sub> , H <sub>2</sub> SO <sub>4</sub> , MgSO <sub>4</sub>
	Zuend & Seinfeld, 2012	O <sub>3</sub>	low	(NH <sub>4</sub> ) <sub>2</sub> SO <sub>4</sub>
limonene	Jaoui et al., 2006	OH, O <sub>3</sub>	high	no seed
	Kundu et al., 2012	O <sub>3</sub>	low	no seed
isoprene	Surratt et al., 2006	OH	high / low	(NH <sub>4</sub> ) <sub>2</sub> SO <sub>4</sub> , H <sub>2</sub> SO <sub>4</sub> , no seed
	Surratt et al., 2010	OH	high / low	(NH <sub>4</sub> ) <sub>2</sub> SO <sub>4</sub> , H <sub>2</sub> SO <sub>4</sub> , no seed
	Lin et al., 2012	OH	high	no seed
	Lin et al., 2013	OH	low	(NH <sub>4</sub> ) <sub>2</sub> SO <sub>4</sub> , H <sub>2</sub> SO <sub>4</sub> , MgSO <sub>4</sub>

998

999 **Table A2.** Properties and kinetic parameters of the VOC oxidation product used in  
 1000 the simulations for SOA growth.

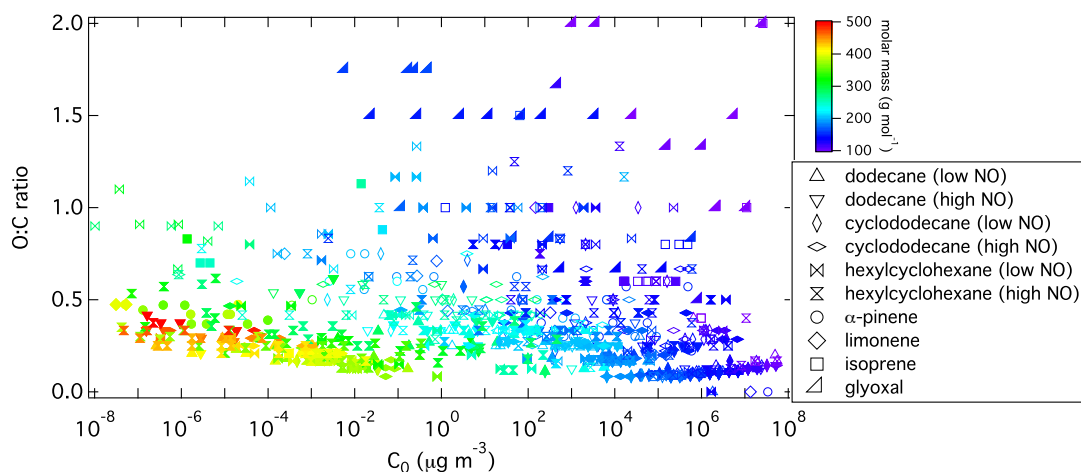
Parameter (Unit)	Description	(a)	(b)	(c)	(d)
$\alpha_{s,0}$	surface accommodation coefficient	1	10 <sup>-3</sup>	1	1
$\tau_d$ (s)	desorption lifetime	10 <sup>-6</sup>	10 <sup>-6</sup>	10 <sup>-6</sup>	10 <sup>-6</sup>
$C_0$ (μg m <sup>-3</sup> )	saturation mass concentration	10 <sup>3</sup>	10 <sup>3</sup>	10 <sup>3</sup>	10 <sup>-3</sup>
$D_b$ (cm <sup>2</sup> s <sup>-1</sup> )	bulk diffusion coefficient	10 <sup>-5</sup>	10 <sup>-5</sup>	10 <sup>-17</sup>	10 <sup>-5</sup>
$D_g$ (cm <sup>2</sup> s <sup>-1</sup> )	gas-phase diffusion coefficient	0.01	0.05	0.05	0.01
$k_g$ (min <sup>-1</sup> )	first-order gas-phase reaction rate coefficient	0.1	0.1	0.1	0.1

1001



1003 **Figure S1.** Atomic O:C ratio vs. volatility ( $C_0$ ) at 298 K for oxidation products of  
 1004 dodecane at low (a) and high (b) NO condition, cyclododecane at low (c) and high (d)  
 1005 NO condition, and hexylcyclohexane at low (e) and high (f) NO condition and  
 1006 isoprene (g),  $\alpha$ -pinene (h), limonene (i), and glyoxal and methylglyoxal (j). The solid  
 1007 and open markers, color-coded with molar mass ( $\text{g mol}^{-1}$ ), correspond to the gas- and  
 1008 particle-phase products, respectively. With a linear regression analysis, the correlation  
 1009 between both quantities has been evaluated (dotted lines) with coefficients of  
 1010 determination ( $R^2$ ), including prediction intervals at the 95 % confidence level  
 1011 (dashed lines).

1012  
 1013  
 1014  
 1015  
 1016



1017  
 1018 **Figure S2.** Summary of O:C ratio vs.  $C_0$  for dodecane, cyclododecane,  
 1019 hexylcyclohexane,  $\alpha$ -pinene, limonene, isoprene, and glyoxal. The solid and open  
 1020 markers, color-coded with molar mass ( $\text{g mol}^{-1}$ ), correspond to the gas- and particle-  
 1021 phase products, respectively.